Technical Evaluation Report
TAACOS: Phase I NUV Report

Date:	2/1/2001
Document Number:	COS-11-0024
Revision:	Revision A
Contract No.:	NAS5-98043
CDRL No.:	N/A

Prepared By:	Steven Penton	10/19/2000
	S. Penton, COS Software Scientist, CU/CASA	Date
Reviewed By:	Ira Becker	11/9/2000
	I. Becker, COS Software Consultant, BATC	Date
Reviewed By:	Dennis Ebbets	[illegible]000
	D. Ebbets, COS Software Consult[illegible] BA[illegible]	[illegible]
Reviewed By:	Stephane Beland	10/23/2000
	S. Beland, COS Softwa[illegible] U/CASA	Date
Approved By:	Ken Brownsberger	10/27/2000
	K. Brownsberger, COS Sr. Software Scienti[illegible]	Date
Approved By:	Jim Green	11/6/2000
	Jim Green, COS Principal Inv[illegible]	Date
Approved By:	Erik Wilkinson	10/26/2000
	Erik Wilkinson, COS Scientist	Date
Approved By:	John Andrews	11/6/2000
	John Andrews, COS Experiment Manager	Date

Center for Astrophysics & Space Astronomy
University of Colorado
Campus Box 593
Boulder, Colorado 80309

REVISIONS

Letter	ECO No.	Description	Check	Approved	Date
-		Initial Release			10/19/00
A	COS-O53	TA with TA1 update			2/01/01

Revision A Name:	Date
Drawn: S. Penton	2-01-01
Reviewed:	
Approved:	

THE UNIVERSITY OF COLORADO

At Boulder

The Center for Astrophysics and Space Astronomy

Technical Evaluation Report

TAACOS: Phase I NUV Report

Size	Code Indent No.	Document No.	Rev
A		COS-11-0024	A
Scale: N/A			

TABLE OF CONTENTS

TABLE OF TABLES

TABLE OF FIGURES

1. SCOPE

The purpose of the Target Acquisition Analysis for the Cosmic Origins Spectrograph (TAACOS, see COS-08-0011) is to ensure that the algorithms and procedures defined in COS OP-01, IN0090-619, IN0090-623 and COS-FSW-001 are sufficient to accurately place a science target of interest at a proper location in the aperture in a timely and efficient fashion. This document focuses upon our TAACOS simulations of target acquisitions (TA) with the COS NUV channel. The TA requirement is that the science target should be aligned to within 45 km/s (~±0.24" for the NUV channel) in the dispersion direction (DD) in the 3σ case for the medium resolution gratings. The NUV XD requirement is only that the target spectra should be fully contained in the predicted detector subarray used in spectral extraction. In the XD, target accuracies of ±0.5" will ensure that no target flux is vignetted by the aperture. An offset error of 22 XD pixels is ~0.5". There exists an additional science requirement of allowing for TAs with accuracies of 15 km/s (±0.08" for the NUV channel, medium resolution) in the dispersion direction in the 3σ case for special observations. Phase I of the NUV TAACOS analysis is designed to provide an initial evaluation for all TA phases for the NUV gratings. The Phase I goal is to determine if the proposed algorithms are viable to center the targets with the desired accuracies. We will also propose improvements to the initial TA strategy, which should allow NUV observations to routinely exceed the stricter 15 km/s accuracy for both dispersion and cross-dispersion target centering. Recommended changes to the flight software (FSW) will be given in COS-11-0014. Phase II of the TAACOS project will expand the targets tested. For further details of the TAACOS project, see COS-08-0011 or http://cos-arl.colorado.edu/TAACOS. This document relies heavily upon the description of the TAACOS FUV Phase I report (COS-11-0016).

1.1 BACKGROUND

HST/COS TAs are planned to be performed spectroscopically without the aid of sky images. This type of TA is more complicated than imaging TAs, and new procedures have been described to spectroscopically acquire targets with COS. To test these new TA procedures a COS simulator has been developed that can produce a detector image for any grating, target location, and input spectra. We will also investigate the use of the TA1 mirror to perform TAs using conventional TA image centering. This document describes the lessons learned from simulating the NUV TA procedures. The simulator and the analysis are performed using ray-tracing and other software developed using the Interactive Data Language (IDL) at CU/CASA. This effort relies heavily on ground-based estimations of the COS in-orbit performance. Final TA algorithms will be tested during the integration and testing (I&T) phase of the COS development.

1.2 NUV PHASE I: PROJECT OVERVIEW/EXECUTIVE SUMMARY

The NUV channel TA has been evaluated for the G185M, G225M, G285M, and G230L gratings. For Phase I of this evaluation, we will restrict our analysis to the acquisition of an isolated quasi-stellar object (QSO) of $F_\lambda = 10^{-14}$ ergs/cm^2/s/Å using the 2.5" diameter primary science aperture (PSA). The redshift of the input spectra was taken to be 0.125. The Phase II analysis, if required, will be performed using both the PSA and the bright object aperture (BOA) at all planned aperture locations. Phase II targets will be varied by redshift, spectral index, and flux. In addition, crowded fields and extended targets will be tested in Phase II. This document describes the Phase I TAACOS evaluation analysis for all four phases of the TA process, Calibrate Aperture Location (LTACAL), Target Search (LTASRCH), Peakup in the Cross-Dispersion Direction (LTAPKXD), and Peakup in the Dispersion Direction (LTAPKD). The acronyms used to describe each of the TA phases are taken from the flight software subroutine names as described in the Control Section Flight Software Requirements Document (IN0090-619).

We find that the original, "stock" (LTASRCH+LTAPKXD+LTAPKD), TA strategies will center isolated point sources to within the required accuracies (0.24"), provided minor adjustments to these routines and strategies are employed. For example, one typical stock TA had 3σ TA errors of 0.13" in the DD and 0.47" in the XD. This equates to a TA introduced 3σ wavelength error of <25 km/s for the medium resolution gratings, and <250 km/s for the G230L. Stock NUV TAs should take less than 20-30 minutes for a $F_\lambda=10^{-14}$ ergs/cm^2/s/Å point source.

We also find that TA using the TA1 mirror (LTAIMAGE) to image a point source on the detector is extremely fast and accurate, provided that the target was initially centered to within 1.7" of the aperture center (4σ errors of <0.01" in both the DD and XD). LTAIMAGE exposures should take less than 5 minutes.

For initial pointing errors greater than 1.7", a 3x3 or 4x4 LTASRCH followed either by a LTAIMAGE or by a LTAPKXD+LTAPKD are the preferred NUV TA strategies. These modes would take from 12-30 minutes for a $F_\lambda=10^{-14}$ ergs/cm^2/s/Å QSO. Unlike the FUV TA's, following up the initial LTASRCH with a second LTASRCH does not improve target centering owing to the much higher detector noise of the NUV MAMA.

We find that flux-centroiding is the best method for the LTASRCH and LTAPKD phases. However, the higher background rate mandates that a "floored'' threshold flux-centroid (FFC) algorithm be used for all LTASRCH and LTAPKD TA steps. Using the mean cross-dispersion coordinate is sufficient in LTACAL and LTAPKXD, although using a median procedure during LTAPKXD would greatly improve TA accuracy in the XD direction. Specifics of the flux-centroid algorithms considered can be found in COS-11-0021. Our recommended flight software (FSW) and operations changes can be found in COS-11-0014.

Extraction subarrays that remove Geocoronal airglow lines are not essential for NUV TA, as there is only one modest line (OI λ2471) in the NUV waveband.

1.3 DOCUMENT OVERVIEW

In §2, we list the applicable COS documentation related to this report. In §3, we list the abbreviations and acronyms used in this document. In §4, we will briefly review the NUV detectors, the coordinate systems used, the HST point spread function (PSF) at the COS science apertures, and current estimates of the COS NUV effective areas. In addition, we describe the input QSO spectrum used for our TAACOS simulations, as well as the TA extraction subarrays used in our TAACOS simulations. In §5, we use our TAACOS NUV simulator to test the four target acquisition (TA) phases (LTACAL, LTASRCH, LTAPKXD, and LTAPKD) independently. In §5, we will discuss the possibility of using the TA1 mirror to perform imaging TAs. In §6, we test the TA phases as a package for fourteen TA scenarios. We test these packages against a range of initial pointing error distributions. In §7, we briefly summarize our NUV TA findings.

2. APPLICABLE DOCUMENTS

The following documentation describes the algorithms and procedures proposed for HST/COS target acquisition. The referenced documents are of the revision in effect on the date of the release of this document

COS-08-0011	TAACOS: Target Acquisition Analysis for the COS (CASA)
COS-11-0014	Recommended Flight Software and Operations Changes based on the TAACOS Phase I Reports for the FUV and NUV Channels
COS-11-0016	TAACOS: FUV Phase I Report
COS-11-0017	TAACOS: Detector TA Summary FUV and NUV Images
COS-11-0021	TAACOS: Recommendations for the TA Flux-Centroiding Algorithm
COS-11-0027	TAACOS: Target Acquisition with the TA1 Mirror
COS-FSW-001	Target Acquisition Concepts for COS (BATC)
COS-NUV-001	NUV MAMA Subsystem Performance
COS-SYS-022	Current Estimates of COS Sensitivity
COS-OP-01	COS Science Operations Requirement Document (CASA)
IN0090-619	Control Section Flight Software Requirements Document for the COS (BATC)
IN0090-623	Software Design Document for the Control Section Flight
ST-ICD-02E	Axial Scientific Instruments to Optical Telescope Assembly and Support Systems Module (STSCI)

3. LIST OF ACRONYMS AND ABBREVIATIONS

ACS	Aperture Coordinate System
BATC	Ball Aerospace & Technologies Corp.
BOA	Bright Object Aperture
BOP	Bright Object Protection
BR	detector Background count Rate
CAL	Calibrate Aperture Location
CASA	Center for Astrophysics and Space Astronomy
CDR	Critical Design Review
COS	Cosmic Origins Spectrograph
CU	University of Colorado @ Boulder
DD	Dispersion Direction (ACS X, DCS Y)
DCS	Detector Coordinate System
FC	Flux Centroid
FFC	Floored (threshold) Flux Centroid
FOS	Faint Object Spectrograph
FSW	Flight SoftWare
FUSE	Far Ultraviolet Spectroscopic Explorer
FUV	Far UltraViolet
FWHM	Full Width at Half Maximum
GSC II	Guide Star Catalog II (STSCI)
HST	Hubble Space Telescope
HVLOW	LOW High Voltage state
HVNOM	NOMinal High Voltage state
IC	Image Coordinate system
IDL	Interactive Data Language
I&T	Integration and Testing
LTACAL	TA subroutine for the Location of the CALibration lamp spectra
LTAPKD	TA subroutine for the PeaKup in the Dispersion direction
LTAPKXD	TA subroutine for the PeaKup in the cross(X)-Dispersion direction
LTASRCH	TA subroutine for target Locating with a (spiral) target SeaRCH
LTAIMAGE	TA subroutine for target Locating with the TA1 mirror
m	minute
MAMA	Multi-Anode Microchannel Array
NUV	Near UltraViolet
p	Pixel
PSF	Point Spread Function (of HST)
PtNe	Platinum-Neon (Wavelength Calibration Lamp)
PSA	Primary Science Aperture
QSO	Quasi-Stellar Object
RTB	Return To Brightest

RVMM	Rear View Mirror Mode (TA1)
s	second
SR	Source (target) count Rate
TA	Target Acquisition
TA1	Target Acquisition 1 (one) mirror
TAACOS	TA Analysis for COS
TS	(Spiral) Target Search
UCB	University of California at Berkeley
X_f	Final ACS DD target location
X_0	Initial ACS DD target location
XD	Cross-Dispersion (ACS Y, DCS X) direction
Y_f	Final ACS XD target location
Y_0	Initial ACS XD target location

4. NUV DETECTOR OVERVIEW AND PERFORMANCE ANALYSIS

4.1 BACKGROUND AND THE NUV DETECTOR COORDINATE SYSTEM

The COS NUV detector is the STIS flight spare band 2 MAMA. The detector is illuminated by three independent camera mirrors, which are part of the NUV optical path (see COS-11-0001). Each of the three mirrors produces a spectral stripe on the detector. Each of the MAMAs 1024x1024 pixels are 25µm on a side. Figure 1 displays the COS MAMA detector coordinate system (DCS), and shows the location of the three science and wavelength calibration stripes. Unlike the FUV DCS, the NUV dispersion direction (DD) is identified as Y and the cross-dispersion (XD) direction is X.

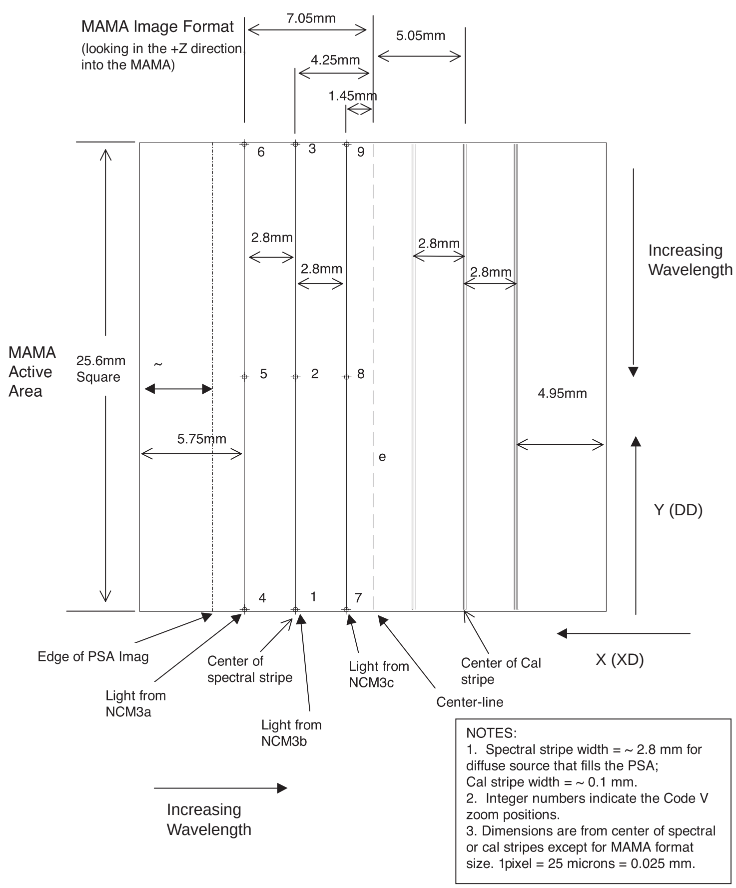

Figure 1: NUV Detector Coordinate System. This figure details the physical locations of the three science and wavelength calibration NUV spectral stripes. This figure was taken from COS-11-0001.

4.2 THE HST POINT SPREAD FUNCTION AND COS SCIENCE APERTURES

As pointed out in the COS-11-0016, the primary driver to the COS TA algorithms is the relationship between the size of the point spread function (PSF) of HST and the COS aperture at the aperture location. Current ray-tracing codes indicate that the on-axis unfocused HST PSF is approximately symmetric with a radius of ~0.204mm (0.75"). Figure 2 displays the HST PSF of a point source at the COS primary science aperture (PSA) in coordinates of millimeters and arcseconds on the sky. The 2.5" diameter aperture is shown in red, simulated photons from an isolated point source are shown in green. The hashed area indicates the aperture mechanism, which blocks photons not in the aperture. The PSA and the bright object aperture (BOA) are both 0.340mm (1.250") in radius. Therefore, the COS science apertures capture 100% of the HST PSF, plus an additional ~0.136mm (0.5") annulus (indicated by Δr in Figure 2). We define the aperture coordinate system (ACS) as having X in the horizontal direction and Y in the vertical of Figure 2. In our ACS, the origin is at the center of the aperture with X increasing to the right and Y increasing upward when looking forward in HST bay 4. In our analysis we will be comparing initial HST pointings in the dispersion direction (DD, X_0) and in the cross-dispersion direction (XD, Y_0) to the final telescope pointings (X_f and Y_f). We will commonly compare the mean of the absolute value of the pointing errors. We designate this as $\langle|X_f-X_0|\rangle$ in the DD and $\langle|Y_f-Y_0|\rangle$ in the XD. Owing the rotation of the detector coordinate system (DCS) to the ACS, ACS X and DCS Y are in the DD, while ACS Y and DCS X are in the XD. In this document, X_0, Y_0, X_f, and Y_f will always refer to ACS coordinates.

The spatial relationship between the COS apertures and the HST PSF limits the accuracy of centering the target at the center of the aperture. For example, an off-axis mis-alignment of 0.5" in any direction will still produce the same number of counts (ignoring Poisson statistics) as a perfectly on-axis TA. TA methods that rely solely upon photon counts, such as flux-centroiding, will have difficulty to properly center a target with accuracies better than 0.5". If the target were off-axis by 0.48" in dispersion and cross-dispersion direction, ~14% of the photons would be vignetted producing a clear indication of target mis-alignment. An example of this configuration was show as Figure 3 of COS-11-0016. These simulations are for a monochromatic point source, and consisted of ~1600 photons. No Geocoronal airglow lines have been included. If included, they would uniformly fill the aperture.

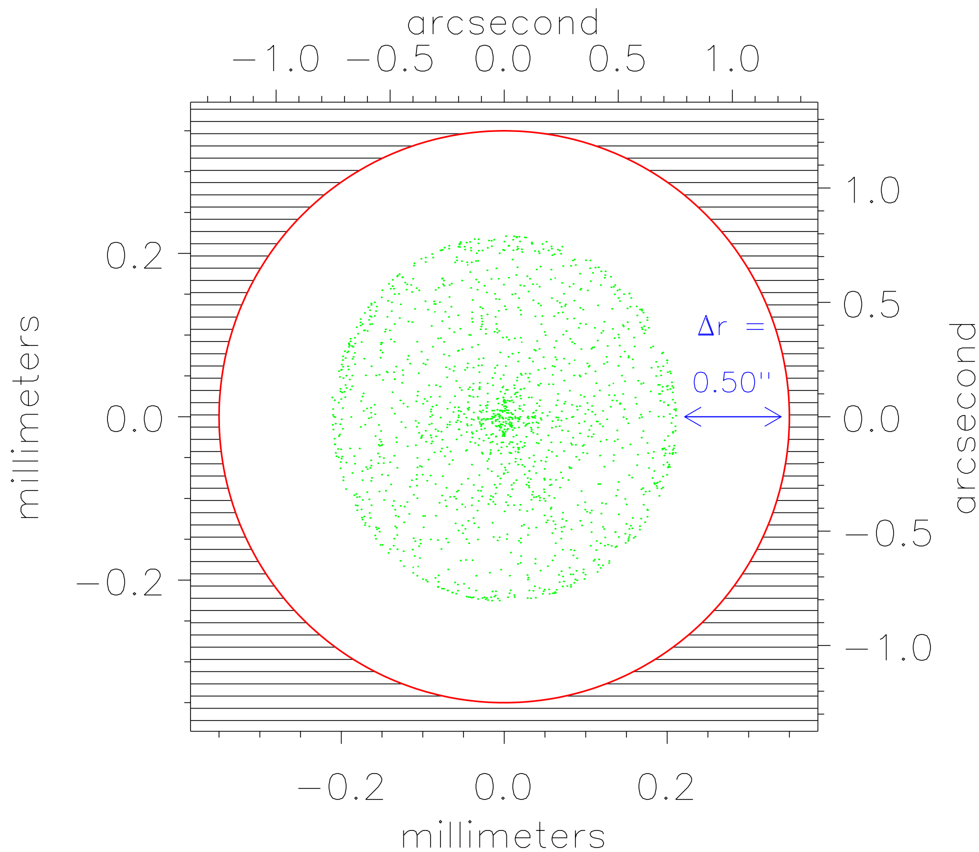

Figure 2: The HST PSF as compared to the COS PSA. The aberrated, out of focus, HST PSF is approximately circular with a radius of ~0.2 mm at the COS aperture mechanism. The COS PSA is circular with a radius of 0.34mm, which corresponds to 1.25” on the sky. The HST PSF is smaller than the COS PSA aperture by 0.136mm or ~0.5”.

4.3 TAACOS: INPUT SPECTRUM

The TAACOS input spectrum for the majority of our modeling is based upon the faint object spectrograph (FOS) QSO composite spectrum (Zheng, et al. 1998, ApJ, 492, 855). The TAACOS NUV input spectrum differs from the FOS QSO composite spectrum in the following ways:

1) It has been scaled to an average flux level of $F_\lambda = 10^{-14}$ ergs/cm^2/s/Å.This is 10 times brighter than the TAACOS FUV target.

2) It has been adjusted to correspond to a target with *z*=0.125.

3) OI λ2471 Geocoronal emission has been added. This line appears in the G225M, G285M, and G230L bandpasses. TAACOS analysis, based upon STIS in-orbit measurements of the strength of the OI λ2471, indicate that NUV TA should not be affected by this weak emission line. Therefore, unlike the FUV channel, no special TA subarrays are necessary to mask out this Geocoronal feature during NUV TA.

4) Simulated non-physical absorption features are inserted into the spectrum at regular intervals ranging from equivalent widths of 2 Å to 2 mÅ. These spectral features are a convenient method for determining the sensitivity limits of COS observations.

Figures 4-6 of COS-11-0016 display the input spectra for the FUV detectors, without Geocoronal lines. The TAACOS NUV spectra are similar, but at higher wavelengths.

4.4 COS EFFICIENCES AND DETECTOR NOISE

The COS instrument (optics + detectors) efficiencies used for the NUV TA analysis are taken from (COS-SYS-022), and are current as of January 27, 2000. For convenience, these efficiency results are presented in Figure 3. Before being processed by the TAACOS simulator, the count rate corresponding to the input flux is determined using the effective area curves and detector background events are added. For purposes of TA, we assume that the detectors will have a constant background rate of 34 counts s^{-1} cm^{-2}. This rate is based upon the in-flight count rate currently being detected by the STIS flight MAMA, corrected for background count rate differences between the nearly identical MAMAs. This count rate equates to 223 counts s^{-1} over the entire detector or about one count per pixel every 78 minutes. This background rate is a factor of 70 higher than the FUV background rate and has important implications regarding NUV TA. Because the effective areas of the NUV gratings are similar at their central wavelengths, we will often chose to display an example of only grating per analysis section.

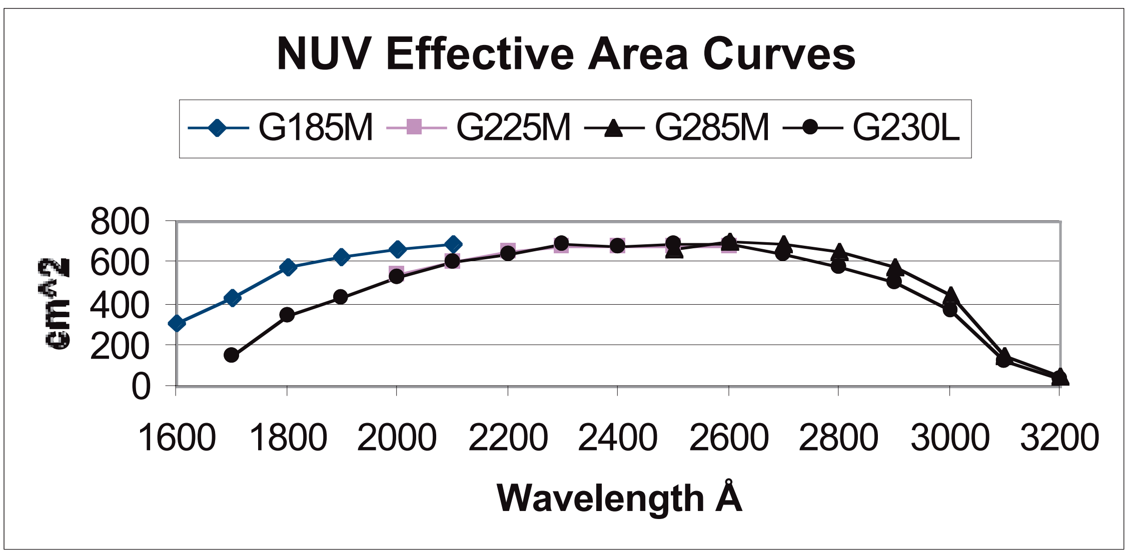

Figure 3: HST+COS NUV effective areas (in cm^2) as a function of wavelength. This figure was taken from COS-SYS-022.

4.5 DETECTOR BLURRING AND EXAMPLE TAACOS NUV SIMULATION

The NUV detectors produce charge clouds that are unique to each incoming photon energy and microchannel plate location. However, this also means that photons of the same energy and location will produce different cloud charges and detector locations. As such, no readout electronics can detect the incoming photon's physical location to better than this intrinsic "blurring". For the COS NUV detectors, the radial blurring is ~32µm FWHM (full width at half-maximum) in both the DD and XD (COS-NUV-001). This intrinsic blurring is added to each incoming photon to create an image of the NUV detector in physical space.

A summary figure for a 30-second exposure time, off-axis (0.5" in ACS X and Y), G185M TAACOS NUV exposure is shown in Figure 4. The input spectrum, described in §4.3, is given in the upper panel. Three spectral sections are color-coded to indicate which spectral stripe they will create on the detector. No Geocoronal airglow lines are expected in this bandpass. The left panel display of the second row displays the detector image (white dashed line) along with the spectral sections of the input spectrum dispersed across the detector. The colored boxes indicate the nominal boundaries of the spectral stripes, and are used as extraction boxes for display purposes. This detector image is displayed in the detector coordinate system (DCS). Note that positive DCS X (XD) is to the left, and positive DCX Y increases upward (DD, decreasing wavelength). The middle panel on the second row shows the full detector with simulated background noise (black) added the blurred photon events. Noise has only been added to the portion of the detector where the spectral stripes can be located. This detector image is displayed in the image coordinate (system) and is in units of pixels. The right panel on the second row shows the HST PSF (green) and COS aperture (red) relationship, and is displayed in the aperture coordinate system (ACS) in both millimeters and arcseconds. Photons landing outside the red aperture circle are vignetted. The third panel shows the TAACOS simulated extracted spectrum for this low S/N observation. Note that there are as many noise events (black) as photon events (blue, green, or red). The bottom panels give the XD profiles for the three spectral stripes in both IC (pixel) and DCS (millimeters), which increase to the left. Note the symmetry of the XD profile of the simulated spectrum versus the uniform detector background. Also note that the +X, +Y ACS off-axis exposure has moved the spectrum in the –X ACS direction.

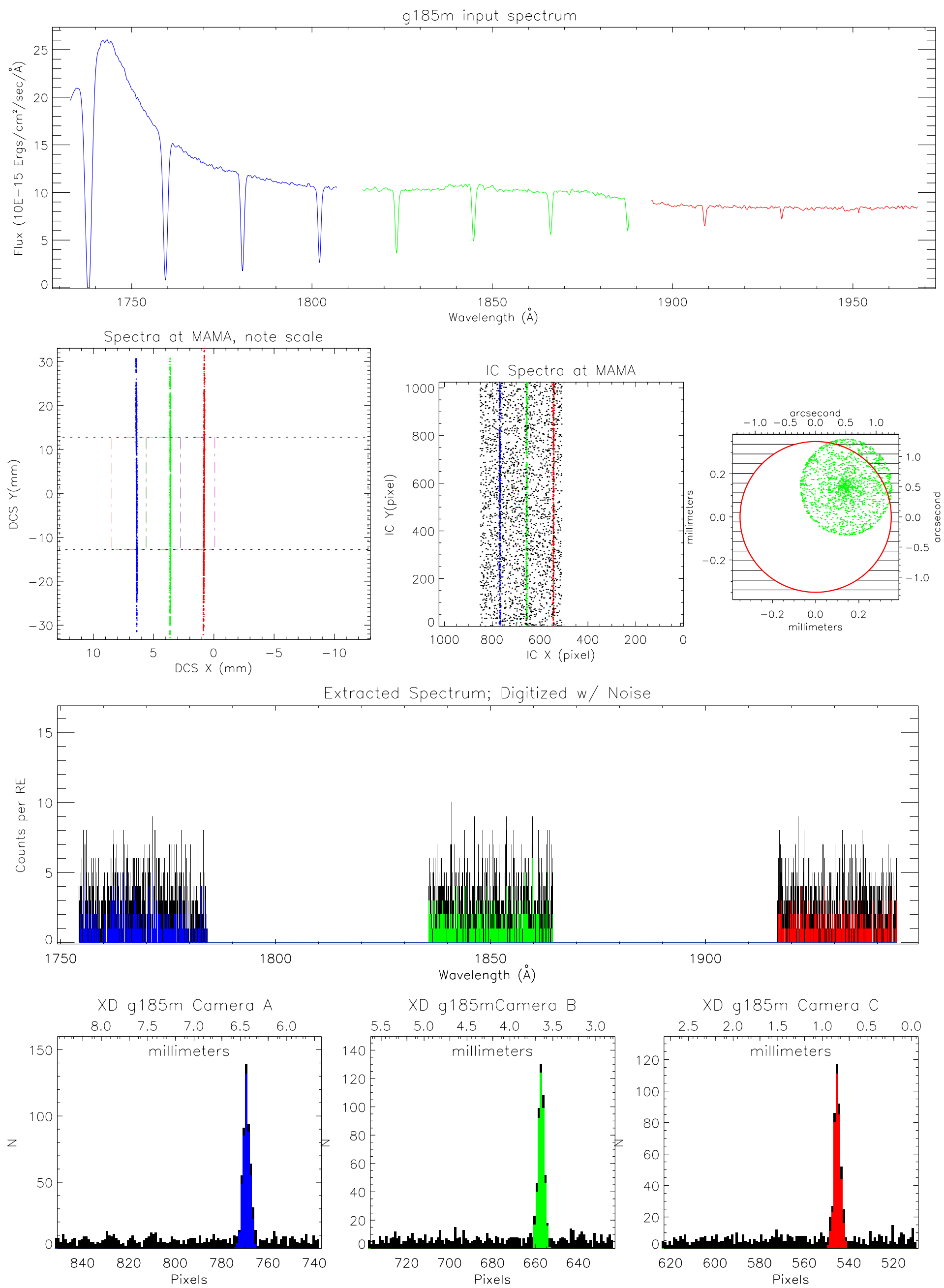

Figure 4: Sample NUV TAACOS simulation. This simulation represents a G185M 30-second exposure of a z=0.125 QSO which is offset by 0.5" in both ACS X and Y. The spectral segments are color-coded throughout the figure, except the HST PSF panel on the second row. In this figure all photons are shown in green. Detector background photons are shown in black.

4.6 DETECTOR PLATE SCALES AND TA EXTRACTION SUBARRAYS

Target motion in the aperture displaces the spectral location on the detector in both the dispersion and cross-dispersion direction. Proper characterization of this motion is necessary for selection of the subarray sizes. To determine this relationship between aperture location and spectral location on the detector, TAACOS simulations were performed using emission line sources displaced over a 7x7x0.4” grid in the aperture. For each grating, the emission line wavelengths were selected near the edges of the bandpasses for each spectral stripe (as in Figure 5). At each grid point, a 4 minute exposure of an $F_{\lambda} = 10^{-14}$ ergs/cm^2/s/Å emission line source was simulated. Background noise simulation was disabled.

The effects of target motion relative to the aperture are displayed in Figure 5. The small figure inset in the upper right displays five target positions relative to the aperture (shown by the black circle). We will refer to this coordinate system as the aperture coordinate system (ACS). The main figure displays the NUV detector in DCS coordinates (both in pixels and physical units). The color-coded dots simulate six emission line locations (two per stripe) based upon the target ACS locations. The dashed lines indicate the boundaries of the three spectral stripes. As indicated by the center, green, configuration, a properly centered exposure places the emission lines in the center of the spectral stripes. Several important issues are displayed in this figure:

1. Target motion in the ACS +X direction produces spectral motion in the –Y DCS direction. For example, tracking from the light blue position to the dark blue location (+X ACS) produces motion on the detector in the –Y DCS direction.
2. Target motion in the ACS +Y direction (i.e. red to light blue) produces DCS motion in the -X direction. However, unlike ACS X-motions, a small amount of +Y DCS motion also occurs (for the medium resolution gratings only).
3. The spectral stripes overlap in DCS X. For example, consider either of the two inner dashed lines. The blue (+Y ACS) emission locations of the leftmost stripe overlap in DCS X with the red (-Y ACS) emission line locations of the stripe to its right.

The rotation indicated by 1 and 2 above is purely due to the choice of coordinate system used to describe the NUV detector. However, the NUV and FUV detectors are similar in respect that an X ACS motion creates spectral motion in the dispersion direction (DD), while Y ACS motion creates spectral motion in the cross-dispersion direction (XD).

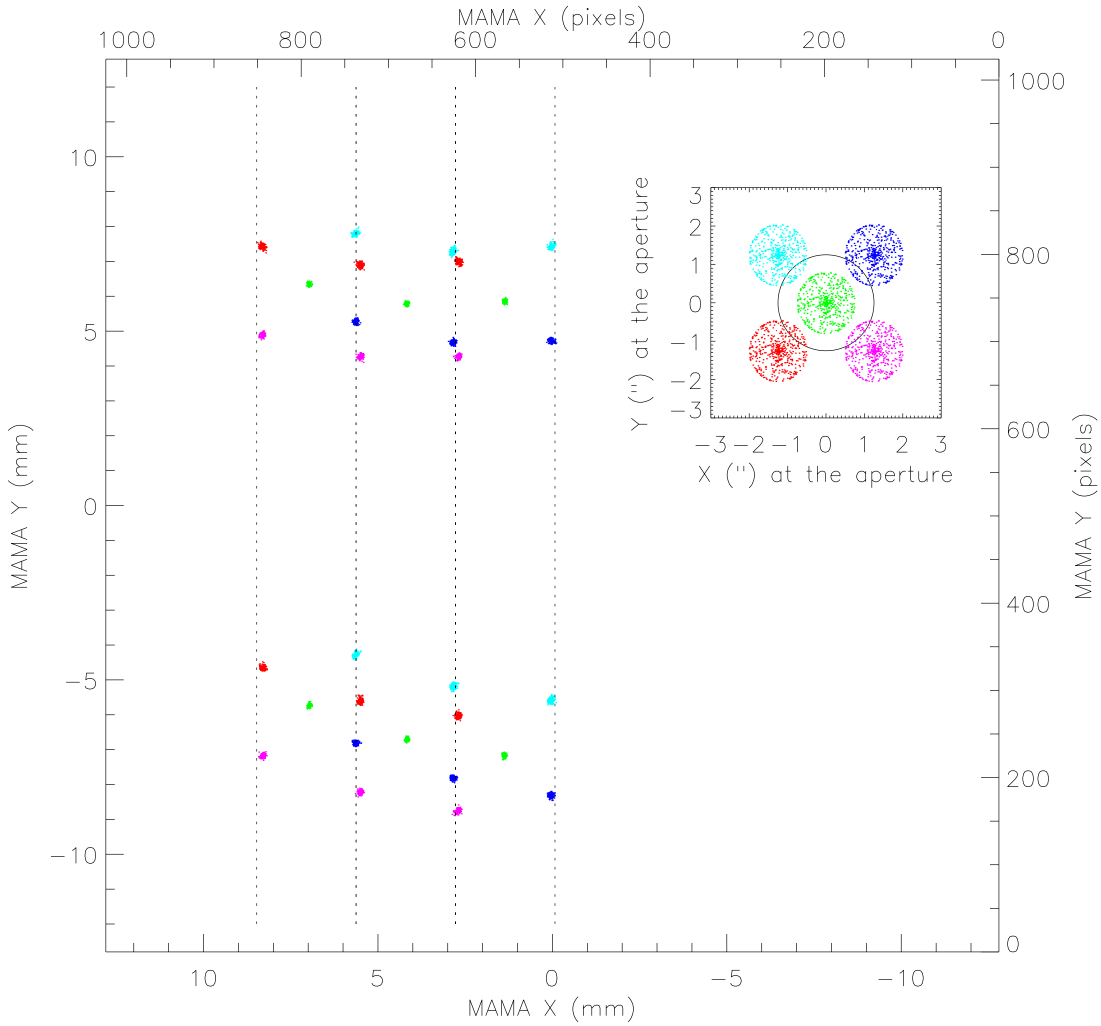

Figure 5: NUV detector map for six emission lines simulated for the five target locations indicated by the inset figure in the upper right. The emission lines and target locations are colored coded. The circle in the inset figure indicates the PSA aperture. The dashed lines in the main figure indicate the approximate spectral stripe boundaries**.**

Of particular concern is the overlap of the spectral stripes. During the LTASRCH phase, there is no information about the location of the target with respect to the aperture. As such, we must create one large extraction subarray to cover the three spectral stripes. In terms of coordinate (X, Y) pixel pairs, one large (513,0) to (847,1023) IC TA extraction subarray would be required for the LTASRCH and LTAPKD phases. In this case, we lose the individuality of the spectral stripes, which is perfectly acceptable during the TA steps that only consider photon counts. For the LTAPKXD phase, the extraction subarray would be focused upon a single stripe and set to exclude any possible region of overlap. This equates to a rectangular extraction subarray of size 51x1024 pixels for the center, 'B', stripe, located approximately at IC (654,0) to (705,1023). The center of other spectral stripes 'A' and 'C' are at IC X (XD) pixel coordinates of 794 and 566, respectively. The actual location of the extraction subarray depends on the results of the LTACAL TA phase (see §4.8 and §4.10). The offset from the median calibration lamp spectrum to the median center of the 'B' is ~ 393p IC X. Figure 6 displays a TAACOS simulation of a uniformly filled aperture for the G225M grating, in the format of Figure 4. The input spectrum is in counts. The color-coded XD profiles show the spectral overlap. As shown in the extracted spectrum panel, these crossover photons were incorrectly wavelength calibrated.

In the FUV TAACOS analysis, the dispersion and cross-dispersion aperture-detector coefficients (α_x and α_y in units of IC pixels (p) per arcsecond (")) were determined by linear least squares fits to the median location of the emission lines in the both directions. However, the TAACOS simulations indicate a slight rotation between aperture motion and detector motion. As such, we have measured the plate scales using four coefficients, α_{xx}, α_{xy}, α_{yx} and α_{yy}, where the first subscript indicates ACS motion, and the second motion on the detector (DCS or IC) motion. Under this scheme, α_{xy} quantifies the amount of DCS Y motion for a given ACS X motion.

To measure these coefficients, the results of all emission lines are combined to produce the final mapping coefficients for each grating. These slopes are a measure of the change of spectral location on the detector for a given translation in the aperture. To produce these coefficients, two planes are fit to the emission line data. Equation 1 describes these planes. In these equations, Δ describes a measured or induced motion in the ACS or DCS coordinate system. The determined values of these coefficients are given in Table1. Error bars are difficult to estimate, but are on the order of a few tenths of a p/".

Equation 1: Planar Aperture Coefficient Mapping Definitions

$$\Delta Y_{DCS} = \alpha_{XY} \Delta X_{ACS} + \alpha_{YY} \Delta Y_{ACS}$$
$$\Delta X_{DCS} = \alpha_{XX} \Delta X_{ACS} + \alpha_{YX} \Delta Y_{ACS}$$

Table 1: Aperture to Detector Mappings

Grating	Dispersion (ACS Y)		Cross-Dispersion (ACS X)	
	α_{xy}	α_{yy}	α_{xx}	α_{yx}
G185M	-42.49 p/"	6.26 p/"	0.02 p/"	-41.85 p/"
G225M	-42.48 p/"	6.19 p/"	0.17 p/"	-41.89 p/"
G285M	-42.47 p/"	6.73 p/"	0.11 p/"	-41.80 p/"
G230L	-42.47 p/"	0.56 p/"	0.01 p/"	-42.27 p/"

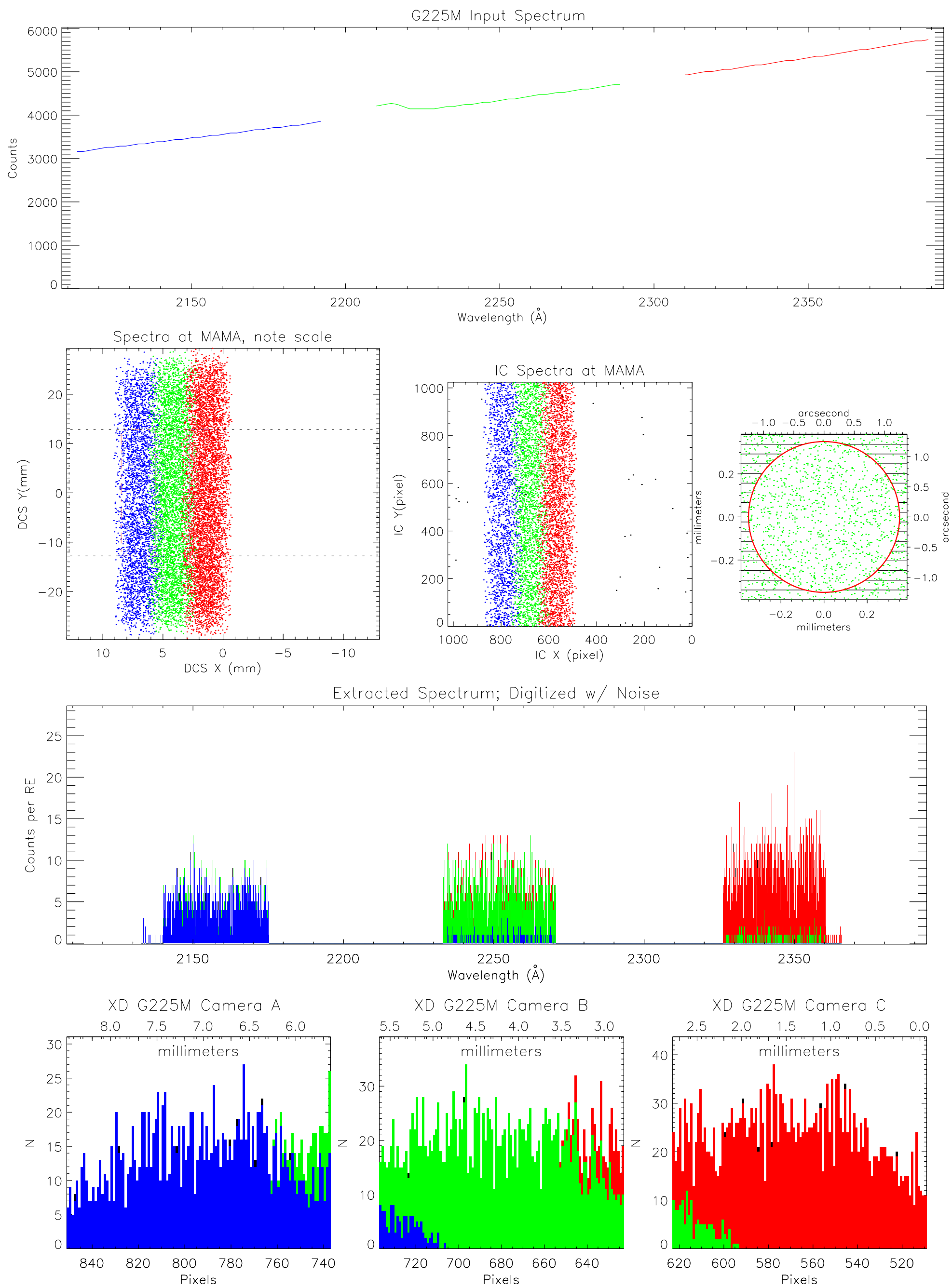

Figure 6: TAACOS simulation of a uniformly filled aperture for the G225M grating, in the format of Figure 4. The upper panel shows the input spectrum in units of counts. Note the overlap of the spectral stripes in the XD profiles.

The +Y DCS spectral motion associated with +Y ACS motion (α_{yy}) is curiously reduced from the G230L trials. The reduced G230L coefficient and the DD nature of the motion imply that this could be related to the dispersive properties of the gratings. Currently, we believe this to be related to the physical orientation of the gratings. Tests are ongoing to further investigate this behavior. We have elected to not include cross-term plate scales in our analysis or algorithms, as we are able to achieve our TA centering goals without complicating the TA algorithms with this second-order correction. For simplicity, we have taken α_{xx} and α_{yy} to be zero, and use the G230L values of α_{xy} for both α_{xy} and α_{yx}. The cross term will introduce a greater than 6 pixel spectral shift for a 1" ACS Y motion. Fortunately, only the XD, α_{yx} coefficients is used in any TA phase (LTAPKXD). This behavior is not seen with the TA1 mirror.

The 0.75" radius of the HST PSF, combined with the 1.25" radius of the COS science apertures implied that a region 2" in radius would be the preferred extraction subarray for LTAIMAGE exposures. This would be implemented by an extraction subarray 4" on a side or 4"*42.5" = 170 pixels on a side.

Once the target is known within the aperture (after LTASRCH), separate TA extraction subarrays for each stripe would be possible. However, given the overlap regions of the stripes, a centering of better than ±0.65" (±25p) would be required for an uncontaminated center stripe LTAPKXD.

We have considered the need for moving extraction subarrays, as was done for the FUV analysis, by examining the situation of a 1pixel wide emission line 1000 times brighter than the continuum that lies just outside the on-axis TA extraction subarray. Suppose that we are flux-centroiding in the dispersion direction using three dwells points of 1.2" offset with an initially on-axis pointing. The central (on-axis) dwell point will receive 1024 counts for an extraction subarray with 1024 pixels. An off-axis pointing of 1.2" places ~60% of the PSF in the aperture. Slewing in one direction will move the strong emission feature into the fixed extraction subarray giving this dwell point 0.6*(1024 + 1000) = 1,214 counts. The other direction will record 0.6*1024 = 614 counts. In this case, the dispersion direction flux centroid would give a pointing error of 0.25". In the less extreme case of an emission line 100 times the continuum the pointing error is 0.03". Therefore, in the vast majority of cases moving subarrays will not be required to achieve our TA accuracy goals. However, in some cases, targets with strong emission lines will cause TA to exceed the TA accuracy goals with fixed subarrays.

4.7 SIGNAL TO NOISE AND EXPOSURE TIMES OF NUV TA EXPOSURES

Unlike the FUV detector, the higher background rate of the NUV MAMA coupled with the large extraction region of many of the TA phases prevents high signal to noise (S/N) TA observations. The TA algorithms will need to be tuned to compensate for this challenge. The source counts (S) to detector background counts (B) ratio, S/B, is not a function of time, but is merely the ratio of the respective count rates. We abbreviate the detector background count rate as BR and the source count rate as SR. For the extraction subarrays recommended for LTASRCH and LTAPKD in §4.6, the BR is 77.8 counts/s. With the G225M grating, our $F_\lambda=10^{-14}$ ergs/cm^2/s/Å source has a SR of 90.8 counts/s. For the smaller LTAPKXD one stripe extraction subarray, the BR is 11.4 counts/s, while for the proposed LTAIMAGE extraction subarray, the BR is 6.5 counts/s. Therefore, for this simulated observation the LTASRCH/LTAPKD, LTAPKXD, and LTAIMAGE phases would have S/B ratios of 1.16, 2.4, and 36.3, respectively, regardless of exposure time.

However, just because an observation has a low S/B ratio does not mean that this target flux (count rate) is not suitable for NUV TA. By choosing appropriate TA algorithms, the target can be acquired as long as a sufficient number of source counts are accumulated. This is possible because the source and background counts have different spatial distributions on the NUV detector. A fiducial limiting count rate can be estimated as the count rate at which three times the Poisson uncertainty of the BR equals the SR. By this definition, the LTASRCH and LTAPKD phases place a lower limit of acquirable targets at $F_\lambda= 3x10^{-15}$ ergs/cm^2/s/Å. On the other hand, the LTAPKXD phase relies upon the XD distribution of flux, and therefore requires that S/B > 1.2 for 0.24" accuracy. This places the lower flux limit for the LTAPKXD phase at $F_\lambda=5x10^{-15}$ ergs/cm^2/s/Å.

The NUV source counts to noise (S/N) ratio is a function of exposure time (T_{exp}). The S/N ratio for the LTASRCH and LTAPKD phases, where a floored threshold is used, would approximately follow the background subtracted S/N ratio indicated in Equation 2. In the LTAPKXD TA phase, the DD columns are collapsed to determine the XD centroid of a single spectral stripe. As shown in §4.5, the XD extent of a spectral strip is ~4 XD pixels (p), while the entire extraction subarray is 51p in XD extent. Under these conditions the S/N per pixel for the LTAPKXD phase is give by Equation 3.

Equation 2: Signal to Noise Ratio of Background Subtracted NUV TA Exposures

$$\frac{S}{N} = \frac{SR * \sqrt{T_{\exp}}}{\sqrt{SR + 2 * BR}}$$

Equation 3: S/N Ratio of LTAPKXD Exposures per XD Pixel (p)

$$\frac{S}{N}(p) = \frac{(SR/4 + BR/51) * \sqrt{T_{exp}}}{\sqrt{\left(\sqrt{SR/4}\right)^2 + \left(\sqrt{BR/51}\right)^2}} = \sqrt{(SR/4 + BR/51) * T_{exp}}$$

Figure 7 shows the exposure times required to reach S/N of 40 and 100 for the LTASRCH and LTAPKD phases, and S/N of 10 and 20 for the LTAPKXD TA phase as a function of mean source flux for the G225M grating. The S/N values are per DD collapsed XD pixel for the LTAPKXD phase and total counts for the other phases. These ratios are indicative of the required S/N to successfully perform the various TA phases. Based upon these exposure times, we will use 30s to simulate all phases of TA using the G225M grating for our $F_{\lambda}=10^{-14}$ ergs/cm^2/s/Å source. Our simulations indicate that this exposure time is adequate for all the medium resolution gratings. Due to its larger bandpass, G230L TA phases for this source would take about 20 seconds.

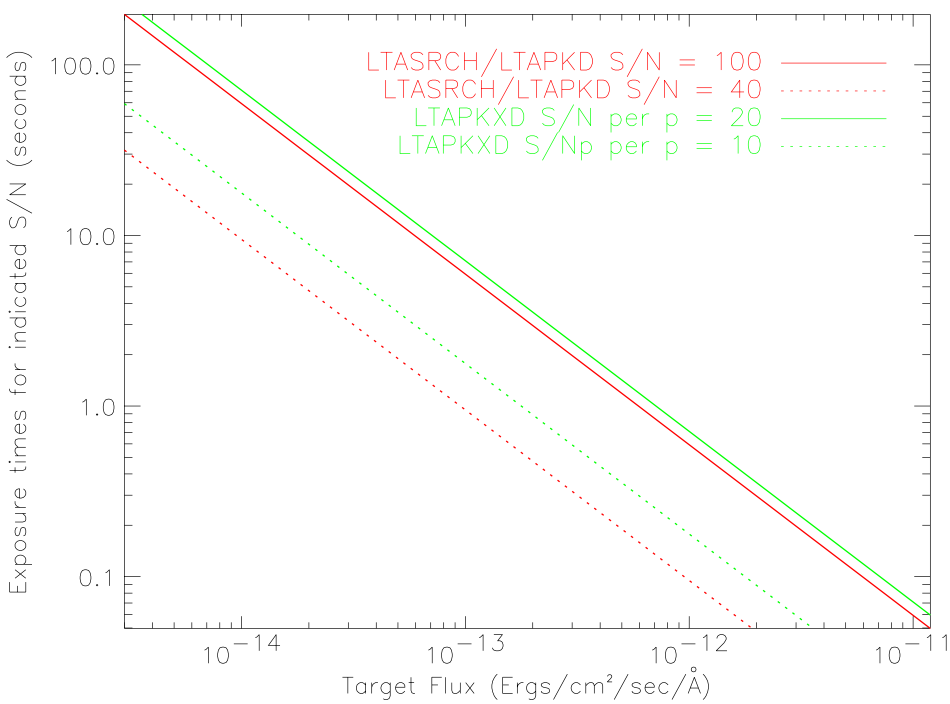

Figure 7: Exposure times required to reach the indicated S/N ratios for the TA phases using the G225M grating. Note that the LTAPKXD S/N is per XD pixel (p) while the LTASRCH/LTAPKD is for the entire TA subarray**.**

ANALYSIS BY TA PHASE

In this section, we examine each of the target acquisition phases described in the document OP-O1. For each phase, we will compare various options and scenarios to determine the efficiency and reliability of the TA phases. For each TA phase, we will also estimate the required execution time. We will report two estimates, one (in seconds(s)) will be our best approximation, and another (in minutes (m)) will be a conservative estimate produced by rounding our best estimates up to the next integer minute. The timing are for our $F_{\lambda}=10^{-14}$ ergs/cm^2/s/Å QSO source. Various assumption are made in producing the timing estimates:

1) The external shutter is closed at the beginning of TA, remains closed during LTACAL, and remains open during all other TA phases,
2) The detector voltage is ramped up from HVLOW to HVNOM at beginning of TA and remains at HVNOM for the duration of TA,
3) All HST slews less than 5" take 40s,
4) All HST slews, other than the initial pointing, are perfect (no pointing error), and
5) All TA phases and procedures are performed sequentially with no overlap.
6) Local count rate (BOP) exposures are performed for every exposure.

We designate the low voltage (down) state of the NUV detector as HVLOW and HVNOM as the nominal (up, high) voltage state for data collection. In addition, we abbreviate the cross-dispersion direction as XD, and the dispersion direction as DD. As previously described, in our analysis we will be comparing initial HST pointings in the dispersion direction (DD, X_0) and in the cross-dispersion direction (XD, Y_0) to the final telescope pointings (X_f and Y_f). HST pointings will always be compared in the ACS.

4.8 CALIBRATE APERTURE LOCATION (LTACAL)

4.8.1 Purpose

The calibrate aperture location procedure (LTACAL) locates the cross-dispersion location of the Platinum-Neon (PtNe) calibration lamp on the detector. Photons from the calibration lamp follow a nearly identical optical path as those of a science observation, but are directed through a different aperture than science targets. Like science exposures, three spectral stripes are produced. We have elected to only measure the XD position of the central stripe. The method works well, and is the recommended TA algorithm. The known offset between the calibration and science apertures allows one to determine the optimum location of the science target in the science aperture based upon the location of the calibration spectrum on the detector. Due to variations in the mechanical position of the grating, it is expected that this procedure will be required for each target acquisition. This TA phase is performed before all other TA phases, and is performed with the external shutter closed.

4.8.2 Analysis

Figure 8 displays the XD profile of the center stripe of a simulated 4s G185M Pt-Ne calibration lamp spectrum. The other gratings and cameras produce very similar results. The S/N of this spectrum is ~10, but this is only a very crude estimate based upon preliminary calibration lamp fluxes. The actual exposure times are likely to be longer (~10s), but less than 30 seconds. Note the asymmetries in the XD profiles due to off-axis nature of the calibration spectra. Extraction subarrays of ±50p (101x1023p) are centered on the expected calibration XD location. For the three spectral stripes, the expected XD median of the spectral stripes occur at IC X pixels 398 (‘A’), 287 (‘B’), and 175 (‘C’).

As outlined in COS-FSW-001, the expected algorithm is to use the mean XD position. We have tested the reliability of using the mean XD position against an algorithm that uses the median pixel location. We find that the difference between the median and mean is less than 3p (0.07” on the sky) all gratings. Smaller extraction subarrays of ±25p decrease this difference to 1p (0.02” on the sky), but would not allow for larger initial offsets due to grating mis-alignment. For our TAACOS simulations we have used the larger extraction subarrays to simulate a worst-case scenario.

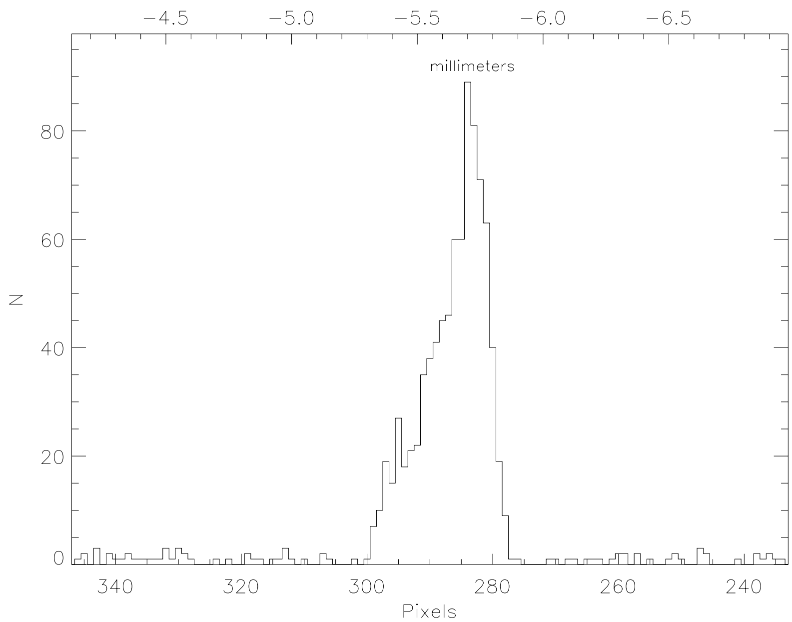

Figure 8: XD profile of a Pt-Ne wavelength calibration lamp G285M exposure. The bottom axis is units of IC pixels, while the upper axis is in physical units (millimeters)

4.8.3 LTACAL Timing

We assume the TA timing begins with LTACAL, after HST has acquired the guide stars and slewed to the approximate position requested by the observer. Assuming that the shutter is closed, and the detector is in a low voltage state (HVLOW) we estimate the LTACAL total time by:

TA FSW initialization	2s
High Voltage Ramp up (HVLOW >> HVNOM)	5s
Calibration Lamp Warm-up	30s
BOP Check	10s
Calibration Lamp Exposure	10s
LTACAL software execution/overhead	5s
LTACAL TOTAL	62s

HVNOM is the nominal (high) voltage state for NUV detector data collection. BOP is the bright object protection check.

4.8.4 LTACAL Conclusions

Despite the obvious asymmetry in the cross-dispersion profile, if narrow TA extraction subarrays are used, the mean and median cross-dispersion pixel values are always within one pixel (this equates to an error of <0.02" on the sky). Only one stripe was used to determine the location of the calibration spectrum. Larger extraction subarrays (±50p) are affected by background counts, and create a larger difference between the mean and median XD coordinate. Use of the median cross-dispersion value is not as sensitive to subarraying, but is much more computationally expensive. For the remainder of TAACOS, we use the mean cross-dispersion method with subarrays that extract ±50p around the nominal cross-dispersion location of the calibration lamp. These extraction subarrays can be seen on the NUV TA summary "cheatsheets" of COS-11-0017. LTACAL should be complete in 62s (or 2m in our conservative estimate).

4.9 TARGET SEARCH (LTASRCH)

4.9.1 Purpose

The spiral Target Search (TS) procedure (LTASRCH) is used to place the science target in the science aperture. Given the initial HST centering accuracy, and the 1.25” radius PSA/BOA, there is no guarantee that the target will be in the aperture after the initial HST pointing. The number of dwell points, the offset distance between each dwell point, and the exposure time per dwell point specifies the spiral TS pattern. The mandatory TS centering accuracy is determined by requiring that the target spectrum is on the detector and is within some known detector subarray appropriate for the subsequent cross-dispersion peakup subarray (LTAPKXD) and dispersion peakup (LTAPKD) TA phases. Simply ensuring that the center of the target PSF is in the aperture satisfies this requirement. Three different center methods will be tested:

1) Return To the Brightest dwell point (RTB),
2) Return to the threshold Flux Centroid of the dwell points (FC), and
3) Return to the threshold “Floored” Flux Centroid (FFC)

The extraction subarray recommended in §4.6 is used during LTASRCH.

4.9.2 Analysis

We find that for the medium resolution gratings, our $F_{\lambda}=10^{-14}$ ergs/cm^2/s/Å input spectrum achieves a S/N ~1 in a 30s exposure. We use this exposure time for each dwell point in the spiral search for the medium resolution gratings. For the G230L exposure we use 20s exposures. In COS-11-0016, we used TAACOS to explore the TS parameter space in terms of the number of dwell points and dwell point offsets. We constructed simulations that compare spiral searches of 3, 4, and 5 dwell points on a side with varying offsets over the range of 0.75-2.3”. We found that the optimum spiral search separation was 1.767” for the FUV. TAACOS simulations indicate that this is also the optimum separation for the NUV.

For our simulations, it is assumed that the initial HST pointing centers the target with a 1σ accuracy of 1". This is consistent with GHRS, FOS, and STIS acquisition histories. The majority of this error is observer error, and is not due to HST’s inability to slew to the proper sky location. It is not expected that TS will be 100% successful, as no TS can recover from errant target coordinates. However, given that COS may be observing the faintest targets ever observed with HST, and therefore the target coordinates may not be well known[1], we should expect to properly center on 3σ (initial slew off by 3”), and

[1] The contrary may actually be true do to the availability of the GSC II catalog and other sky surveys. If this is actually the case, the TA strategies should be optimized for a smaller radius search.

preferably 4σ cases. Our sample was forced to 3% of the trials outside the 3σ circle.

Table 2 gives the G285M results for 100 LTASRCH simulations for the three algorithms tested. The algorithms were tested for 5 dwell point offsets ranging from 1.7-1.8". All other gratings produce very similar results. Our FC algorithm only considers dwell points with a minimum number of counts (16) that are also greater than 10% of the brightest dwell point. Our FFC algorithm subtracts the lowest number of counts in any dwell point from all dwell point counts before applying the FC algorithm, and effectively reduces the number of dwell points by at least one. A "floored" flux-centroiding algorithm is used for STIS TSs. The details of the flux-centroid algorithms that we have considered with TAACOS can be found in COS-11-0021 and COS-11-0014. Table 2 gives the mean and standard deviation of the LTASRCH centering accuracies for both the DD ($<|X_f-X_0|>$) and XD ($<|Y_f-Y_0>$). As before, X_f and Y_f designates the final pointing, in the ACS, while X_0 and Y_0 designate the initial ACS target locations. This table also gives the worst cases (WC) for each of the 100 target acquisitions trials. For the patterns tested, the worst cases are dominated by the initial pointing offsets that lie outside the centers of the edge TS dwell points. These points also drive the reported standard deviations of the mean acquisition errors.

Results of our TAACOS suggest the use of a FFC is mandatory for NUV LTASRCHs. As shown in Table 2, the FFC algorithm always produces better results that the RTB algorithm, which always produces better results than the FC algorithm. The reason for this is the higher detector background of the NUV MAMA. By subtracting off the number of counts in the lowest bin, the FFC effectively applies a background subtraction before the FC. As with the FUV tests, the optimum offset appears be near 1.767"

The 4x4 FFC LTASRCHs produced better results than the 3x3s. For most initial pointing offsets, the target is contained within the center 2x2 pattern. The flooring of the dwell counts therefore usually removes one of the outer dwell points from the FC, preserving the symmetry of the FC where most of the counts remain. When applied to the3x3 pattern, the FFC introduces a slight asymmetry in the FC, causing the results to be slightly worse.

TAACOS simulations indicate that TS can routinely center point sources to within ±0.4" (3σ) in both XD and DD, provided the floored flux-centroid algorithm is used.

Table 2: LTASRCH Results for the G285M Grating

N Offsets	Offset	Return to Brightest			
		$<\lvert X_f-X_0\rvert>$	WC_X	$<\lvert Y_f-Y_0\rvert>$	WC_Y
4x4	1.800"	0.48±0.29"	0.89"	0.51±0.25"	0.90"
4x4	1.775"	0.48±0.28"	0.87"	0.50±0.25"	0.89"
4x4	1.750"	0.47±0.28"	0.89"	0.49±0.25"	0.88"
4x4	1.725"	0.46±0.28"	0.88"	0.49±0.25"	0.90"
4x4	1.700"	0.45±0.28"	0.86"	0.48±0.24"	0.86"
3x3	1.800"	0.42±0.30"	1.06"	0.41±0.30"	1.50"
3x3	1.775"	0.42±0.30"	1.08"	0.41±0.29"	1.52"
3x3	1.750"	0.42±0.30"	1.11"	0.41±0.30"	1.55"
3x3	1.725"	0.42±0.30"	1.13"	0.41±0.30"	1.57"
3x3	1.700"	0.41±0.30"	1.16"	0.40±0.29"	1.60"

N Offsets	Offset	Threshold Flux Centroid			
		$<\lvert X_f-X_0\rvert>$	WC_X	$<\lvert Y_f-Y_0\rvert>$	WC_Y
4x4	1.800"	0.71±0.68"	2.61"	0.58±0.58"	3.07"
4x4	1.775"	0.70±0.68"	2.60"	0.57±0.58"	3.08"
4x4	1.750"	0.71±0.68"	2.60"	0.58±0.58"	3.08"
4x4	1.725"	0.71±0.68"	2.62"	0.57±0.58"	3.08"
4x4	1.700"	0.70±0.68"	2.60"	0.58±0.58"	3.11"
3x3	1.800"	0.67±0.67"	2.68"	0.55±0.58"	3.24"
3x3	1.775"	0.68±0.67"	2.70"	0.55±0.58"	3.26"
3x3	1.750"	0.67±0.68"	2.71"	0.55±0.58"	3.27"
3x3	1.725"	0.67±0.69"	2.72"	0.55±0.58"	3.27"
3x3	1.700"	0.67±0.68"	2.73"	0.55±0.58"	3.29"

N Offsets	Offset	Floored Threshold Flux Centroid			
		$<\lvert X_f-X_0\rvert>$	WC_X	$<\lvert Y_f-Y_0\rvert>$	WC_Y
4x4	1.800"	0.11±0.09"	0.42"	0.13±0.15"	0.82"
4x4	1.775"	0.10±0.10"	0.41"	0.10±0.11"	0.74"
4x4	1.750"	0.11±0.11"	0.51"	0.11±0.15"	0.99"
4x4	1.725"	0.10±0.13"	0.75"	0.10±0.14"	0.96"
4x4	1.700"	0.11±0.17"	0.96"	0.10±0.19"	1.15"
3x3	1.800"	0.15±0.25"	1.41"	0.13±0.27"	1.91"
3x3	1.775"	0.15±0.31"	1.57"	0.12±0.27"	1.87"
3x3	1.750"	0.15±0.28"	1.28"	0.13±0.40"	2.85"
3x3	1.725"	0.15±0.33"	1.60"	0.12±0.37"	2.58"
3x3	1.700"	0.14±0.29"	1.58"	0.12±0.43"	3.05"

4.9.3 LTASRCH Timing

LTASRCH consists of a series of HST slews plus one additional slew after calculating the FC of the TS. For even numbered TSs (i.e. 4x4), one additional slew is required before initiating the spiral search, unless the current FSW routines are modified.

For each dwell point, the required time is:

BOP Check	10s
LTASRCH Exposure for a $F_\lambda=10^{-14}$ ergs/cm^2/s/Å source	30s (20s for G230L)
HST Slew to next location (or FC if last)	40s
LTASRCH calculation/overhead	5s
LTASRCH each dwell point	85s (75s for G230L)

After the last dwell point:

LTASRCH FC calculation/overhead	5s
LTASRCH after last dwell point	5s

Table 3 gives the timing estimates for 2x2, 3x3, 4x4, and 5x5 searches as calculated (in seconds) or rounded up to the next minute for all NUV gratings. Before the LTASRCH phase, the external shutter must be commanded open from the ground.

Table 3: LTASRCH Duration Estimates

LTASRCH Pattern	Exposure Time (ET) Calculation for M Gratings (G230L)	ET as calculated (seconds)		ET rounded up (minutes)	
		M Gratings	G230L	M Gratings	G230L
2x2	85s (75s)*4 +40s +5s	385	345	7	6
3x3	85s (75s)*9 + 5s	770	680	13	12
4x4	85s (75s)*16 + 40s + 5s	1405	1245	24	21
5x5	85s (75s)*25 + 5s	2130	1880	32	32

4.9.4 LTASRCH Conclusions

There are an infinite number of dwell point number and offsets that will achieve the desired result of ensuring that the target is in the aperture, assuming that the TS extent is large enough to sample the PSF center. Targets outside the edge centers of the TS pattern can be centered to no better then the distance from the PSF center to the closest TS pattern dwell point. TS patterns that do not sample the PSF will, obviously, fail. This can happen if the number and offsets of the TS are too small, or if the offsets are so large (>2.8") that the entire PSF falls in a TS pattern hole. The offset of 1.767" is the offset at which diagonal dwell points just overlap (the largest offset without any holes). There appears to be a large offset "sweet spot" between 1-2" in which all TS patterns achieve offset errors of less than 0.2" in the DD and 0.1" in the XD direction. The errors always approach their minimum value near the 1.767" offset. Therefore, unless one wishes to increase the offset solely for the purpose of extending the search area, 1.767" consistently appears to be near the center of the LTASRCH offset "sweet spot" for all trials. LTASRCH offsets greater than 2" should be avoided. At this offset, and greater, it is possible for only one TS dwell point to sample the PSF, introducing error into the FC calculation. It should be noted that some of the LTASRCH trials listed Table 5 already approach, and some exceed, the TA acquisition goal of 0.1" (3σ) in both XD and DD.

Specifically, the 5x5x1.767" trial appears to meet the TA goals by itself, without the aid of the other TS phases. Furthermore, this pattern fully samples a 2x1.767" = 3.53σ initial error offset range. However, this phase takes ~31-35 minutes. As will be demonstrated in the following sections, performing the smaller 3x3 or 4x4 searches, followed by other TA routines can exceed the results of this trial in less time, while sampling the same area.

4.10 PEAKUP IN THE CROSS-DISPERSION DIRECTION (LTAPKXD)

4.10.1 Purpose

The peakup in the cross-dispersion direction (LTAPKXD) is intended to improve the centering of the science target in the direction perpendicular to the dispersion. If the LTASRCH phase was previously successfully executed, the target is ensured to be in the aperture. This guarantees that the target spectrum will be within a known subarray on the detector, but it may not be in the optimum cross-dispersion location. The TAACOS implementation focuses only upon the center NUV stripe. The TAACOS LTAPKXD TA subarray does include the overlap region between the spectral stripes. The LTAPKXD procedure will measure the cross-dispersion location of the spectrum and attempt to move the telescope to place the target in the center of the aperture in the cross-dispersion (XD) direction. The initial approximate location of the spectrum is known from the LTACAL phase. The same LTACAL algorithms for determining the cross-dispersion location of the LTACAL spectrum (mean and median) will be compared in locating the XD center of the target spectrum during the LTAPKXD testing. For the median values, the spectral stripes are located at +396, +393, and +391 IC X pixels with respect to the corresponding wavelength calibration stripes. To ensure that the entire HST PSF is contained within the COS PSA or BOA, targets will need to be centered to within ±0.5” in the XD. Spectral stripe confusion occurs when targets are off-axis by more than ±0.65”. Under these circumstances, the spectral stripes fall on the detector in ambiguous DCS X locations (The center stripe of –0.65” ACS Y target will fall onto the same detector location as an outer stripe of a +0.65” ACS Y observation). To avoid this, the TA extraction subarrays outlined in §4.6 are employed. These extraction subarrays are 51p IC X (XD) by 1024p IC Y (DD) centered on the expected XD location of the spectral stripe. Ideally, the LTAPKXD routine should be able to achieve the same requirements as the DD requirements, a 3σ XD pointing error of ±0.24”. However, merely achieving the ±0.5” XD error requirement 100% of the time is satisfactory in the sense that no target flux is vignetted by the aperture.

4.10.2 Analysis

To test the LTAPKXD procedure, a 7x7x0.13” pointing error grid was used to simulate the HST pointing parameter space expected after a successful LTASRCH. This grid is shown in Figure 9. In this figure, the HST PSF is shown in green, the extent of the PSA/BOA in red, and the 7x7x0.13” grid is shown in blue. The input QSO spectrum is placed at each indicated position, and then the LTAPKXD procedure is executed. For each grating, exposure times of 10s, 20s, 40s, and 60s were measured to determine the mean and median XD coordinate. These results are summarized in Figure 10. In this figure, mean results are shown in green and median results are shown in red. Solid lines indicate the mean or median XD pointing errors after LTAPKXD. Standard deviations about the mean and median are also shown. The XD errors after performing LTAPKXD are non-Gaussian in our pattern trial, therefore we will not consider the 3σ errors, merely the maximum XD pointing error after performing LTAPKXD over our ±0.4” grid. The dashed lines indicate these maximum XD pointing errors after performing LTAPKXD. Note that in our trials, the detector background rate and the target flux are approximately the same (S/N ~ 1.1). Therefore, this trial is close to a worst-case scenario. Note that the XD errors do not decrease with increased exposure time. Unlike the FUV XD profiles, off-axis and dispersion axis variance of the cross-dispersion profile does not affect the LTAPKXD procedure. The higher NUV background does however affect the accuracy of the NUV LTAPKXD procedure. Because the background counts are distributed uniformly across the detector, the median XD coordinate always gives a more accurate centering than does the mean algorithm.

After performing LTAPKID, the XD error is less than 0.2” for the mean algorithm for initial pointing errors < 0.4”. For the median algorithm, the maximum pointing error is less than 0.03” for the same initial distribution. For comparison, these maximum errors equate to approximately 8.4 and 1.3 XD pixels for the mean and median algorithms, respectively.

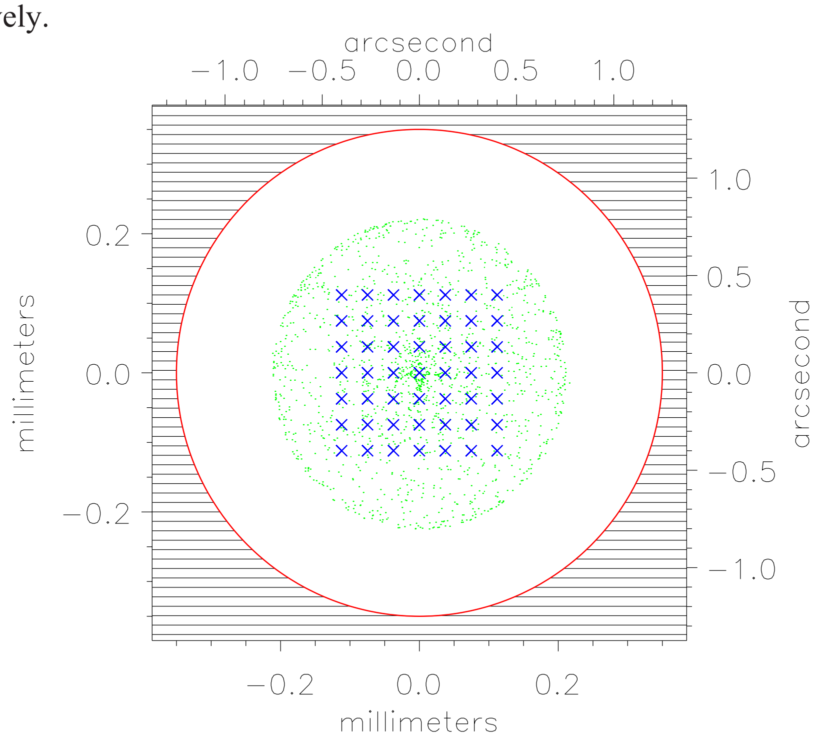

Figure 9: Test Grid for LTAPKXD. The COS PSA/BOA is indicated by the red circle. The HST PSF at the PSA/BOA is shown in green. The 7x7x0.13” test grid for LTAPKXD is shown in blue. A point source is placed at each position indicated, and the LTAPKXD routine is applied to the detected spectrum.

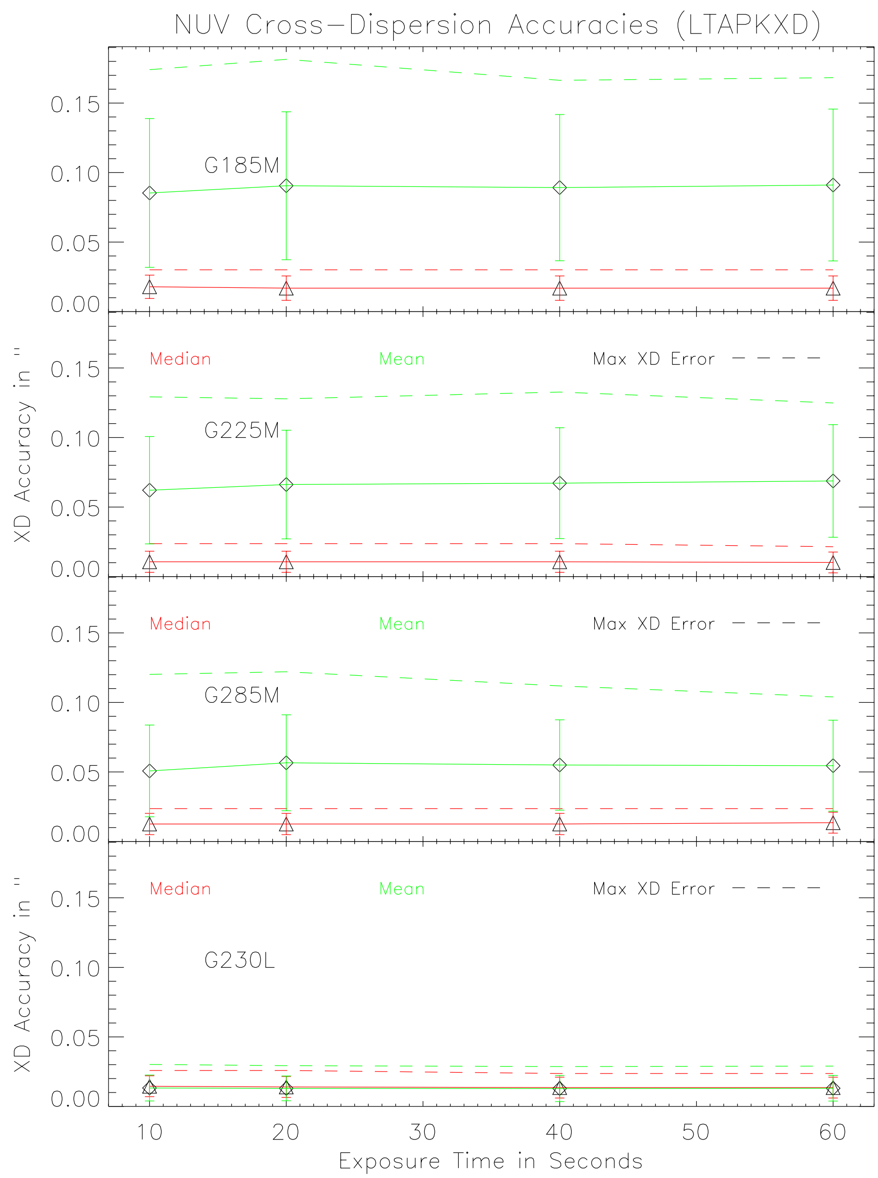

Figure 10: LTAPKXD TAACOS tests results. The mean XD recovery error (in arcsecond) is plotted versus exposure time for our input spectrum for the test pattern shown in **Figure 9**. Each panel corresponds to a given NUV grating. XD coordinates recovered using a mean algorithm are shown in green, the median results are shown in red. The dashed lines indicate the maximum XD error after LTAPKD for the given trials. Standard deviations about the mean and median are shown as error bars. For all trials, the maximum XD recovery error is less than 0.2” for the mean algorithm, and less than 0.03” for the median algorithm (for initial positioning offsets of < 0.4”).

4.10.3 LTAPKXD Timing

BOP Check	10s
LTAPKXD Exposure for a $F_{\lambda}=10^{-14}$ ergs/cm^2/s/Å source	30s (20s for G230L)
LTAPKXD software execution/overhead	5s
LTAPKXD slew	40s
LTAPKXD TOTAL	85s (75s for G230L)

4.10.4 LTAPKXD Conclusions

When using the mean XD location, the LTAPKXD TA phase achieves the ±0.24" XD error for initial pointing offsets of up to 0.4" in both XD and DD for all gratings, provided appropriate TA subarrays are used. Our test case, a $F_{\lambda}=10^{-14}$ ergs/cm^2/s/Å source, only produces a S/B (ratio of source counts to background counts) of ~1.14. This ratio is not a function of time and is the limiting factor in accurately determining the XD location of the NUV spectral stripe. Using the median XD coordinate gives much better accuracy than the mean algorithm (maximum error < ±0.03" for all gratings). This is sufficiently better to warrant considering the addition of a FSW routine for its calculation. It should be noted that the final XD TA accuracy is the combination of the LTACAL accuracy plus the calculated LTAPKXD offset. This TA phase should take at most 2 minutes for an $F_{\lambda}=10^{-14}$ ergs/cm^2/s/Å source.

It should be noted that during LTAPKXD alignment, the target would be moved in ACS Y. As determined in §4.6, ACS Y motions will also cause the spectrum to move in the DCS Y direction. Therefore, it is recommended that the LTAPKXD procedure be performed before the LTAPKD.

4.11 PEAKUP IN THE DISPERSION DIRECTION (LTAPKD)

4.11.1 Purpose

The LTAPKD TA procedure is intended to improve the centering of the science target in the dispersion direction (DD). This TA phase uses an algorithm designed to maximize flux at the detector. This differs from the LTAPKXD phase that positions the spectrum on the detector. In LTAPKD, HST is moved through a series of DD dwell points. The number and sky separations of dwell points are TBD. In LTAPKD, only the total flux within a specified subarray is needed to determine the best telescope pointing. As with the LTASRCH procedure, the algorithms to be tested are:

1) Return to the brightest dwell point (RTB),
2) Return to the flux-weighted centroid (FC) of the dwell points, and
3) Return to the flux-weighted centroid after the number of counts in the lowest count dwell point has been subtracted from the number of counts in each dwell point (a floored flux centroid, FFC).

Since this is also a photon counting algorithm, the same TA subarray was used in this procedure as was used for the LTASRCH analysis

4.11.2 Analysis

To test the LTAPKD TA phase, we used an identical 7x7x0.13” target offset grid used in the LTAPKXD testing (Figure 9). We tested LTAPKD for 3, 4, 5, 7, and 9 dwell points with maximum DD offsets of ±1.5”. The setup for the 5x0.8” LTAPKD trial is shown in Figure 11. In this figure, the HST PSF is shown in green at the center of the search pattern, and the colored x’s correspond to the aperture positions of the same color. Even number dwell points were centered on the initial target location.

Figures 12-15 show the FC and FFC results of our simulations for the four NUV gratings. In all cases, FC and FFC results were superior to RTB centering (not shown in the figures). For all gratings, the FFC results are better for dwell point numbers of three and higher. As previously mentioned this is due to the higher background rate of the NUV detector. The best results were obtained for a FFC using 9x0.375” offsets. FC’s with higher number dwell points suffered from asymmetries in the FC pattern, skewing the final centering towards the middle of the pattern. The FFC algorithm partially alleviates this problem by eliminating the farthest removed dwell point from the FC calculation. FFC’s with fewer than five dwell points introduced asymmetries into the pattern, reducing the LTAPKD centering accuracy.

Due to the magnitude of the plate scale cross-term α_{yy}, it is recommended that the LTAPKXD procedure be performed before the LTAPKD. The LTAPKD procedure will move the target in the ACS X direction, but will not move the target in DCS X.

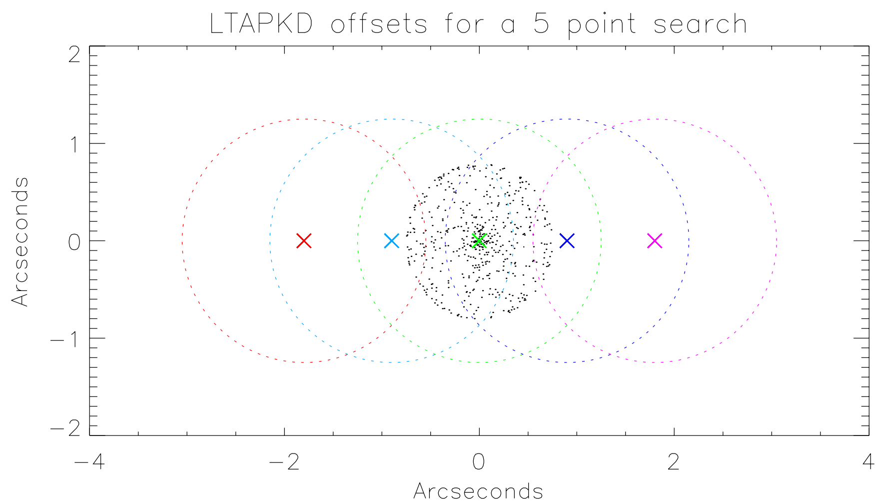

Figure 11: LTAPKD offsets for a 5x0.8" dwell point search. The colors of the aperture extents correspond to the dwell point center colors (x's). The HST PSF at the PSA/BOA is shown at the center dwell point location.

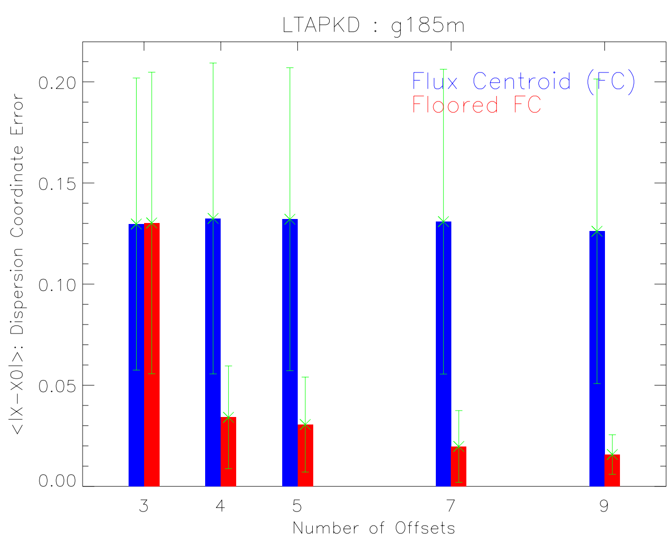

Figure 12: G185M LTAPKD test results. A 7x7x0.13" grid (Figure 9) was used to simulate target positions after performing a LTASRCH target search. Blue bars indicate the mean DD coordinate error after performing the LTAPKD procedure using a flux centroid (FC) algorithm to calculate the target location in the aperture. Standard deviations are indicated in green. Red bars give the results for a floored FC algorithm.

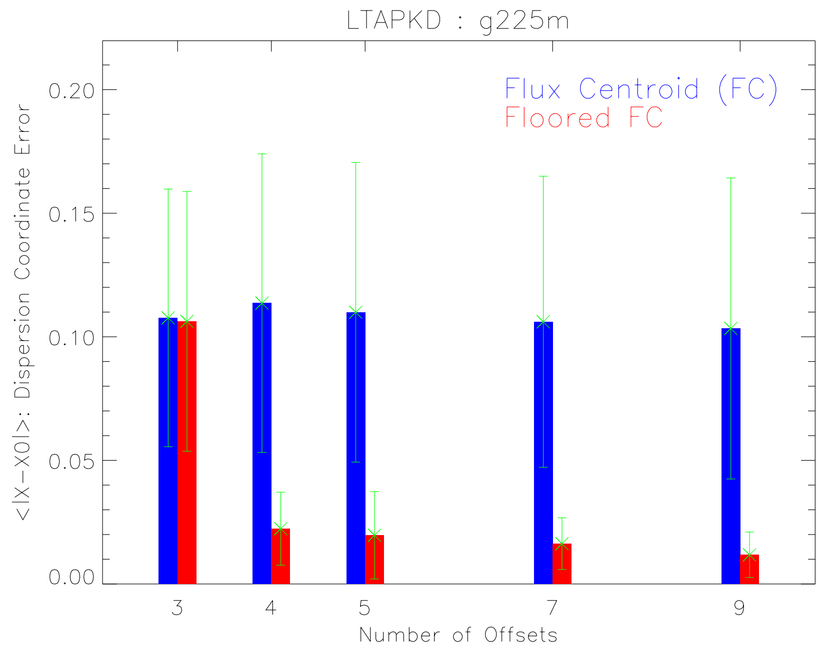

Figure 13: G225M LTAPKD test results. See Figure 12 for description.

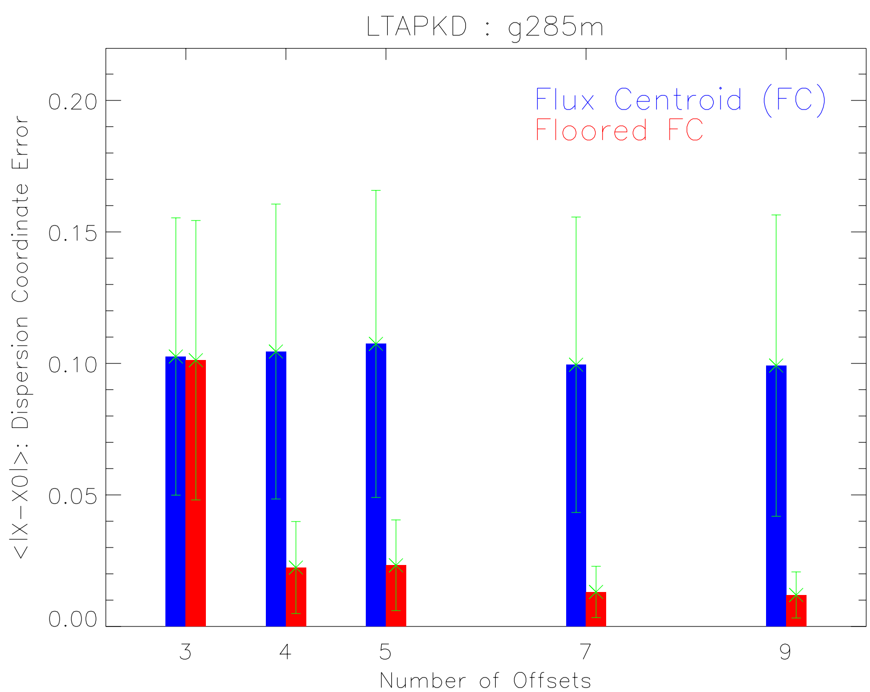

Figure 14: G285M LTAPKD test results. See Figure 12 for description.

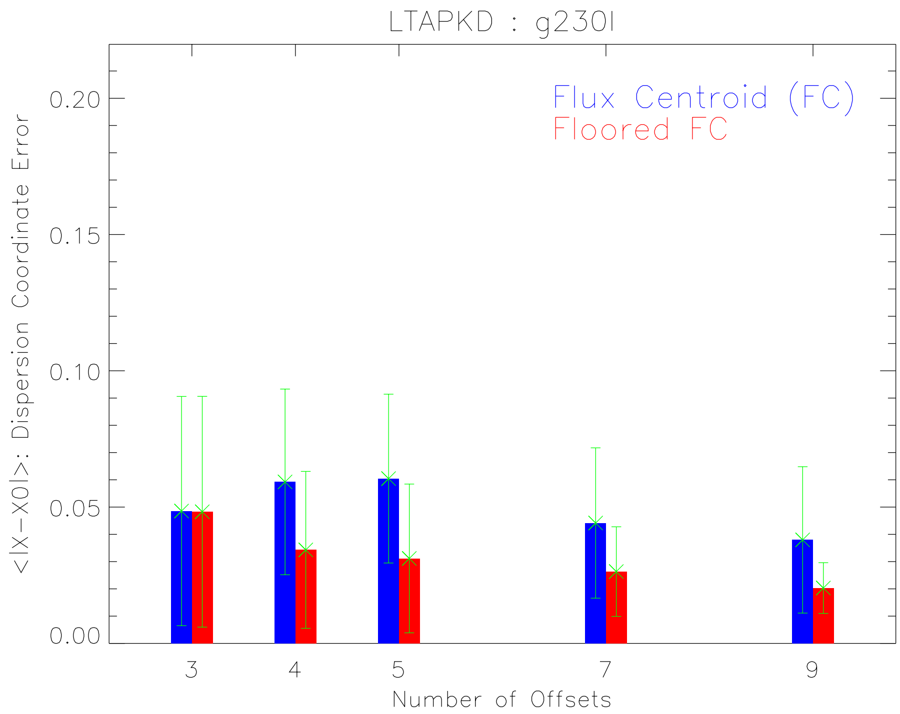

Figure 15: G230L LTAPKD test results. See Figure 12 for description

4.11.3 LTAPKD Timing

Assuming that the external shutter is open, and the NUV detector is in the HVNOM state, each LTAPKD dwell point should take:

BOP Check	10s
LTAPKD Exposure	30s (20s for G230L)
LTAPKD slew	40s
LTAPKD calculation/overhead	5s
Total	85s (75s for G230L)

In addition, we allot 5s for final LTAPKD FC calculation. Therefore a five dwell point LTAPKD would take (5x85s)+5s = 425s (375s for G230LM), or 8m (7m for the G230L) using our conservative round up to the next minute scheme.

4.11.4 LTAPKD Conclusions

All LTAPKD patterns achieve the minimum 0.24" centering accuracy with ease. Some grating and LTAPKD pattern combinations achieve the stricter 0.08" at the 3σ level. The use of the floored threshold flux centroid (FFC) algorithms were superior to the return to brightest centering results or FC methods. The best LTAPKD centering accuracy is achieved using a 9x0.45" FC pattern, however a pattern with only 5 dwell points does almost equally well and takes about half the time. We estimate that this TA phase (with a five dwell point grid) will take 350s for the medium resolution gratings (400s for G185M), or 6m (6m for the G185M) using our conservative estimate. For our test grid, this produced mean DD centering accuracies ($<|X_F-X_0|>$, ACS) of 0.03". Accuracies and standard deviations using a FFC 5x0.8" grid for each grating are given in Table 4 below.

Table 4: LTAPKD results for a 5x0.8" grid.

GRATING	$<\|X_F-X_0\|>$
G185M	0.031± 0.023"
G225M	0.020±0.017"
G285M	0.023±0.017"
G230L	0.031±0.027"

5. LTAIMAGE: TARGET ACQUISITION USING THE TA1 MIRROR

The use of the TA1 mirror to perform TA is explored further in COS-11-0027. Please see this document for updated information, analysis and algorithms. See COS-11-0014 Rev A for our updated recommend TA1-TA algorithms.

5.1.1 Introduction

TA using an image of the sky is possible with COS using the TA1 mirror on OSM2 to image the sky on the MAMA. We call this operation LTAIMAGE. In this, our initial analysis, we are only interested in determining the practicality of this mode. This operation is theoretically limited to sources within a 2” radius of the center of the aperture. This maximum distance, 2”, is the distance from the center of the aperture where photons reach the detector (1.25” radius aperture + 0.75” radius PSF). Operationally, LTAIMAGE works well out to initial radial offsets of up to 1.7”. Once the plate scale, the relationship between arcseconds (“) on the sky and pixels (p) on the detector, and the detector location of a perfectly centered point source are known, LTAIMAGE is a simple calculation of the location of the target image on the detector and one HST slew. The calculation of the center of the target image could be simply based upon the mean or median pixel value or a more complicated algorithm could be employed. Future TAACOS work could be undertaken to optimize this procedure if LTAIMAGE is determined to be a supported COS TA mode.

5.1.2 Analysis

Using the methods for 4.6, we determine the TA1 plate scales to be α_{xy}= -42.57 ± 0.01p/” and α_{yx}= -42.48 ± 0.01 p/”. The other plates scales α_{xx} and α_{xy} are very small (<0.03p/”), indicating that these terms are mainly introduced by the gratings. These plate scales imply the TA extraction subarray for LTAIMAGE would be a square, ~170p on a side. Figure 17 displays a 1s TA1 image for two $F_{\lambda}=10^{-14}$ ergs/cm^2/s/Å QSO sources separated by 1” in both ACS X and Y. The stronger (rear) detection is perfectly centered in the aperture.

The HST+COS+TA1 configuration has a maximum effective area of 1000 cm^2 over a large wavelength range from 1600-3200 Å. The effective area curve for this configuration is shown in Figure 16.

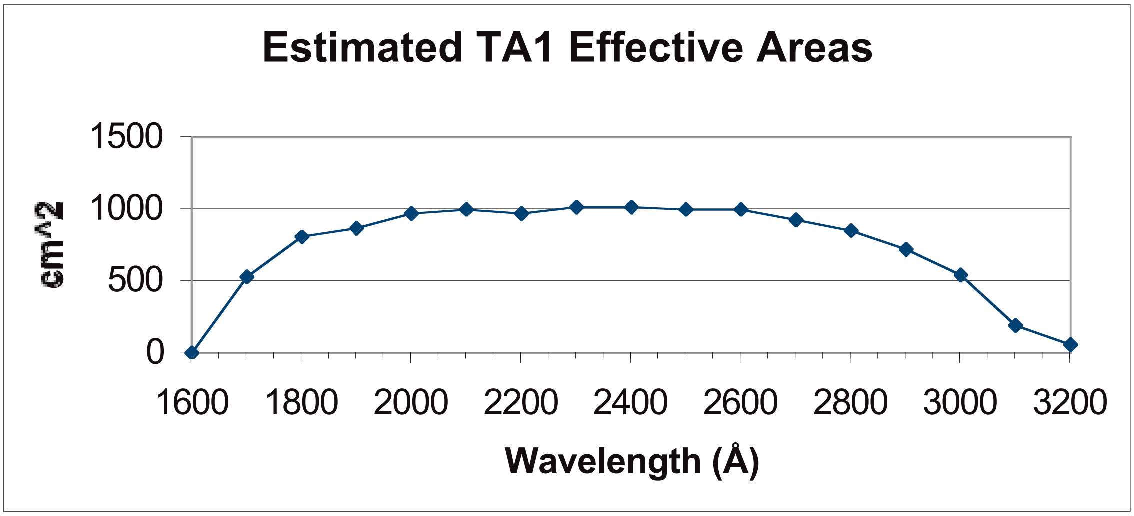

Figure 16: HST+COS+TA1 effective area (in cm^2) as a function of wavelength. This figure was taken from COS-SYS-022.

A major concern when using this non-dispersed mode is the overillumination of the NUV MAMA. There exist two count rate restrictions for the NUV. One is a global limit of 10^6 counts/s over the entire detector. The other, local, limit is 200 counts/s/p. The central pixel of a TA1 image of our sample QSO spectrum achieves this count rate at the mean flux level of approximately $F_\lambda=1.3\times10^{-14}$ ergs/cm^2/s/Å. Because of the uncertain flux and variability of astrophysical targets, the exposure times used for LTAIMAGE should be conservative. As such, we adopt a stricter local limit 100 counts/s/p in our analysis; however, this count rate is probably still too large. For targets brighter than $F_\lambda=1.3\times10^{-14}$ ergs/cm^2/s/Å, two methods of flux attenuation are possible. The first is to position the target in the bright object aperture (BOA). This aperture has a neutral density filter that attenuates flux by a factor of 100. Alternately, the "rear view mirror" mode (RVMM) of the TA1 mirror can be used (COS-11-0001). This mode also attenuates flux by about a factor of 25. Because it does not involve routine motion of the aperture mechanism, it is assumed that targets above a certain count rate will be attenuated with the RVMM, while targets brighter could be attenuated with both the BOA and RVMM. Figure 18 displays estimated maximum count rates for the brightest pixel in the TA1 image for mean fluxes in the range of $F_\lambda=10^{-17}$-10^{-10} ergs/cm^2/s/Å, assuming a maximum local count rate limit of 100 counts/s/p. The green line indicates the maximum count rates for un-attenuated observations. Fluxes exceeding 100 counts per second (dashed green line) are attenuated with the RVMM (display in red), while fluxes that exceed the count rate limit by 2500 are attenuated by both the BOA and RVMM (displayed in blue). Sources with mean $F_\lambda > 6 \times 10^{-10}$ ergs/cm^2/s/Å would not be observable with the TA1 mirror.

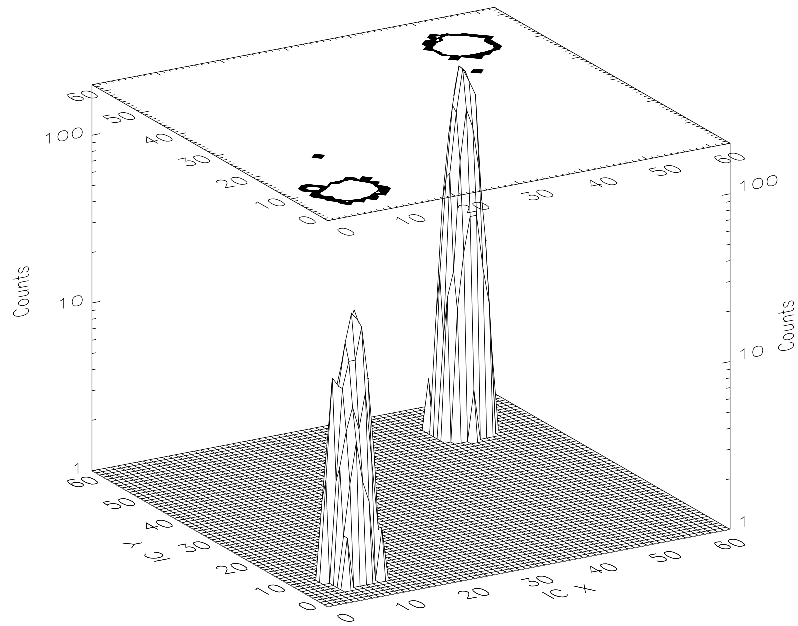

Figure 17: TA1 image of two point sources. The stronger one is centered in the aperture, while the weaker one is offset 1" in both ACS X and Y, and is partially vignetted.

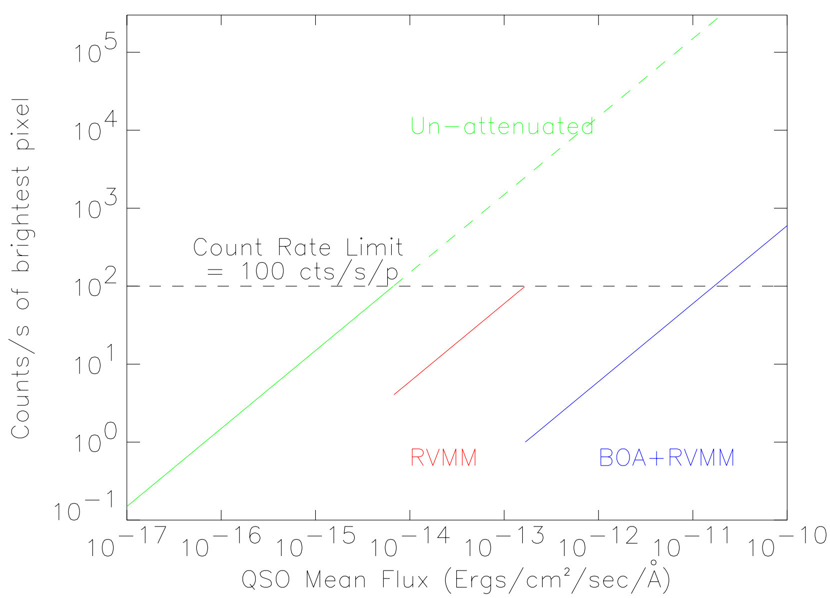

Figure 18: LTAIMAGE count rates versus mean target flux. Count rates that exceed 100 counts/s/p (dashed green line) are attenuated with either the RVMM or BOA+RVMM.

The local count rate limit has serious consequences on the S/N of the TA1 image. The S/N of the TA1 image is calculated by Equation 2. The estimated background count rate (BR) for a 170px170p extraction subarray is ~6.4 counts/s. In Figure 19, we display the exposure time required to achieve S/N of 40 and 100 for the flux ranges obtainable with LTAIMAGE, assuming a local count rate maximum of 100 counts/s/p. In this figure, exposure times (in seconds) required to achieve S/N=40 are shown as dashed lines, while the solid lines represent S/N=100 exposure times. A target whose initial offset is 1" observed at S/N=100, will suffer a 0.01" error in pointing due to background noise (0.025" for S/N=40). Exposure times in green are un-attenuated; those in red and blue have been attenuated by RVMM and BOA+RVMM respectively.

Based upon our analysis, we conclude that LTAIMAGE appears to be a viable addition to the TA arsenal. However, further analysis is required to optimize the LTAIMAGE algorithms and parameters.

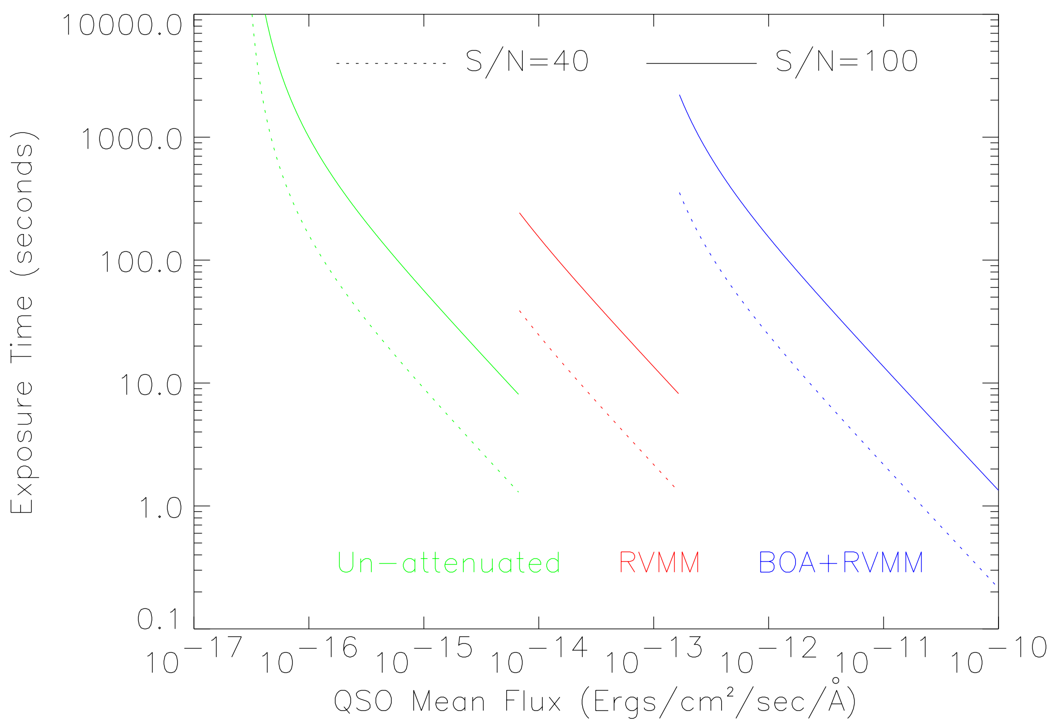

Figure 19: Required LTAIMAGE exposure times. This figure displays the required exposure times to achieve S/N of 40 (dashed) and 100 (solid) over the available LTAIMAGE source flux range. Exposure times in green are un-attenuated; those in red and blue have been attenuated by RVMM and BOA+RVMM respectively.

5.1.3 LTAIMAGE Timing

Assuming that the external shutter is open, and the NUV detector is in the HVNOM state, a LTAIMAGE should take:

BOP Check	10s
LTAIMAGE Exposure	1-1000s
LTAIMAGE slew	40s
OSM2 rotation	120s
LTAIMAGE software execution	5s
Total	176-1175s (2-19m)

LTAIMAGE searches could take anywhere from 176s up to well over 1000s, depending on the flux of the target and S/N of the observation. For most applications, the LTAIMAGE exposure time would average about 100s. Using this exposure time, a typical LTAIMAGE exposure would take ~275s. Our estimate of 120s for an OSM2 rotation is the maximum allowable as described in COS-SYS-012 Rev A (Optics Select Mechanism 2 Requirements).

5.1.4 LTAIMAGE Conclusions

The proposed LTAIMAGE TA mode is extremely fast and accurate. However, caution must be exercised to not exceed the local count rate limit for the MAMA. Accurate knowledge of the integrated flux from 1700-3200Å is important for a successful LTAIMAGE TA. Attenuation with the RVMM and BOA+RVMM modes allow this procedure to be used for sources over a large range of fluxes.

6. COMPARISION OF TA STRATEGIES

In this section, we will compare various TA strategies for a $3\sigma=3''$ initial pointing error distribution. Although historically, a $3\sigma=3''$ distribution is what we might expect for COS observers based upon past HST initial pointings, new digital sky catalogs such as the GSC II may enable COS observers to submit target coordinates more consistent with a $3\sigma=1''$ distribution. Additionally, some observers may know the coordinates of their targets at within 1" (e.g. the target has previously been observed with HST) or they may not need wavelength accuracies of 15 km/s (e.g. a QSO observer may wish to align the Galactic absorption features to the local standard of rest (LSR) as opposed to the heliocentric wavelength scale provided by HST). All comparisons are for our $F_\lambda=10^{-14}$ ergs/cm^2/s/Å QSO source.

6.1 COMPARISON OF TA STRATEGIES FOR A $3\sigma=3''$ DISTRIBUTION.

To compare the various TA strategies, we consolidated all possible TA scenarios down to fourteen strategies that appeared most promising from initial TAACOS simulations. These fourteen scenarios were tested against a population of initial pointing errors that was a combination of a $3\sigma=3''$ Gaussian distribution, plus a more uniform (4σ) component of approximately equal strength to build up number statistics at higher initial pointings errors. The DD distribution of initial target positions is shown in Figure 20. The fourteen scenarios tested were:

```
1) 4x4 LTASRCH (FFC) + 2x2 LTASRCH (FFC) (4x4+2x2)
2) 3x3 LTASRCH (FFC) + 2x2 LTASRCH (FFC) (3x3+2x2)
3) 2x2 LTASRCH (FFC) + 2x2 LTASRCH (FFC) (2x2+2x2)
4) 2x2 LTASRCH (FC) (2x2)
5) 3x3 LTASRCH + LTAPKXD + LTAPKD (3x3+XD+DD)
6) 3x3 LTASRCH + LTAPKD + LTAPKXD (3x3+DD+XD)
7) 4x4 LTASRCH + LTAPKXD + LTAPKD (4x4+XD+DD)
8) 3x3 LTASRCH + LTAPKXD (median) + LTAPKD (3x3+XD (median)+DD)
9) 3x3 LTASRCH + 2x2 LTASRCH (FC) (3x3+2x2nof)
10)   3x3 LTASRCH (3x3)
11)   LTAIMAGE (TA1)
12)   2xLTAIMAGE (2xTA1)
13)   4x4 LTASRCH + LTAIMAGE (3x3+TA1)
14)   3x3 LTASRCH + LTAIMAGE (4x4+TA1)
```

The cumulative distribution results of these simulations are presented Figure 20. In this figure, the left axis gives the percentage of TA's which achieve $<|X_f-X_0|>$ (top, DD) and $<|Y_f-Y_0|>$ (bottom, XD) within the target search error indicated by the bottom axis in arcseconds. As before, X_f designates the final pointing and X_0 the initial ACS target location in the dispersion direction (DD). Similarly, Y designates the cross dispersion (XD) direction. These cumulative distributions are a good measure of the overall TA accuracies as measured by TAACOS. The inset plot in the bottom panel gives the actual initial pointing distribution (X_0 vs. Y_0), and the 3σ (3”) radius is shown in red.

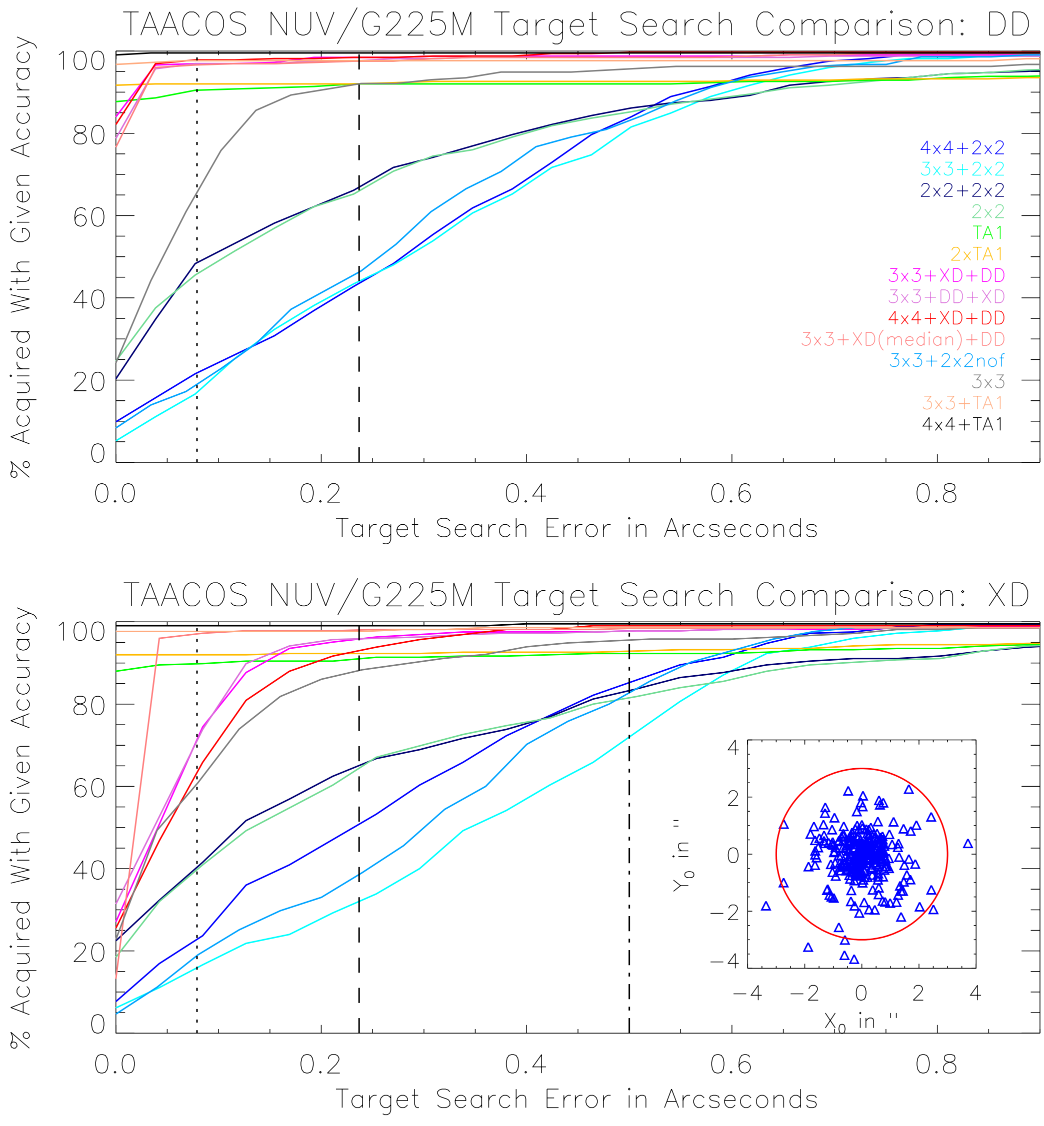

Figure 20: Comparison of TA strategies for a 3σ=3" distribution. TA’s were simulated for an $F_\lambda=10^{-14}$ ergs/cm^2/s/Å QSO acquired with the G225M. Left axis gives the percentage of TA’s which achieve <$|X_f-X_0|$> (top, DD) and <$|Y_f-Y_0|$> (bottom, XD) within the target search error indicated by the bottom axis in arcseconds. The sky distribution of initial target positions is shown in the inset plot. The 3σ=3” area is indicated by the red circle. Vertical dashed lines indicate the various TA accuracy requirements of 0.08”, 0.24”, and 0.5” (XD only).

Several NUV TA lessons can be learned from Figure 20:

- All of double spiral search scenarios fail to properly align the target in both the DD and XD. This is not surprising due to the use of follow-up 2x2 LTASRCHs. Using the FC method on a S/N ~1 observation implies that the FC will always be pulled to the center of the search pattern due to the uniform distribution of background counts over the dwell points. Use of a FFC does not greatly improve the effectiveness of 2x2 LTASRCHs. With the FFC, the symmetry of the 2x2 pattern is broken by the removal of one of the dwell points. In fact, these affects are so severe that the application of a second 2x2 spiral search actually causes the target alignment to worsen.
- The use of a median algorithm during the LTAPKXD phase greatly improves the accuracy in the XD direction
- The LTAIMAGE procedures are excellent in centering the target. The centering failures in the TA1 and 2xTA trials are due to initial pointing which do not place the target with 2" of the aperture center. The use of an LTASRCH before a LTAIMAGE is an excellent way to expand the search area before performing a LTAIMAGE.
- When combined with an LTASRCH, the LTAPKD procedure does an excellent job centering targets in the DD.

To test the spatial extent of the various TA strategies, Figure 21 plots the accuracy extents of the fourteen tested TA strategies for the 3σ=3" distribution. The bottom axis gives the initial pointing errors versus the recovery percentages within 0.08" for the DD (top), XD (middle) and radial dimension ($<|R_f-R_0|>$). The results are smoothed by a 1" moving boxcar filter. In some cases, the recovery rates are exactly the same (usually 100%), so some strategies are difficult to track in this figure. As expected, all TA strategies fall off in centering accuracy as the initial pointing error exceeds the offset where the HST PSF no longer yields any counts in the LTASRCH dwell point search pattern. The double spiral search patterns often fail for targets that are initially well centered. Some anomalies in Figure 21 are due to initial point errors of large radial, but small DD or XD coordinate (the initial pointing error is small in one dimension, but large in the other).

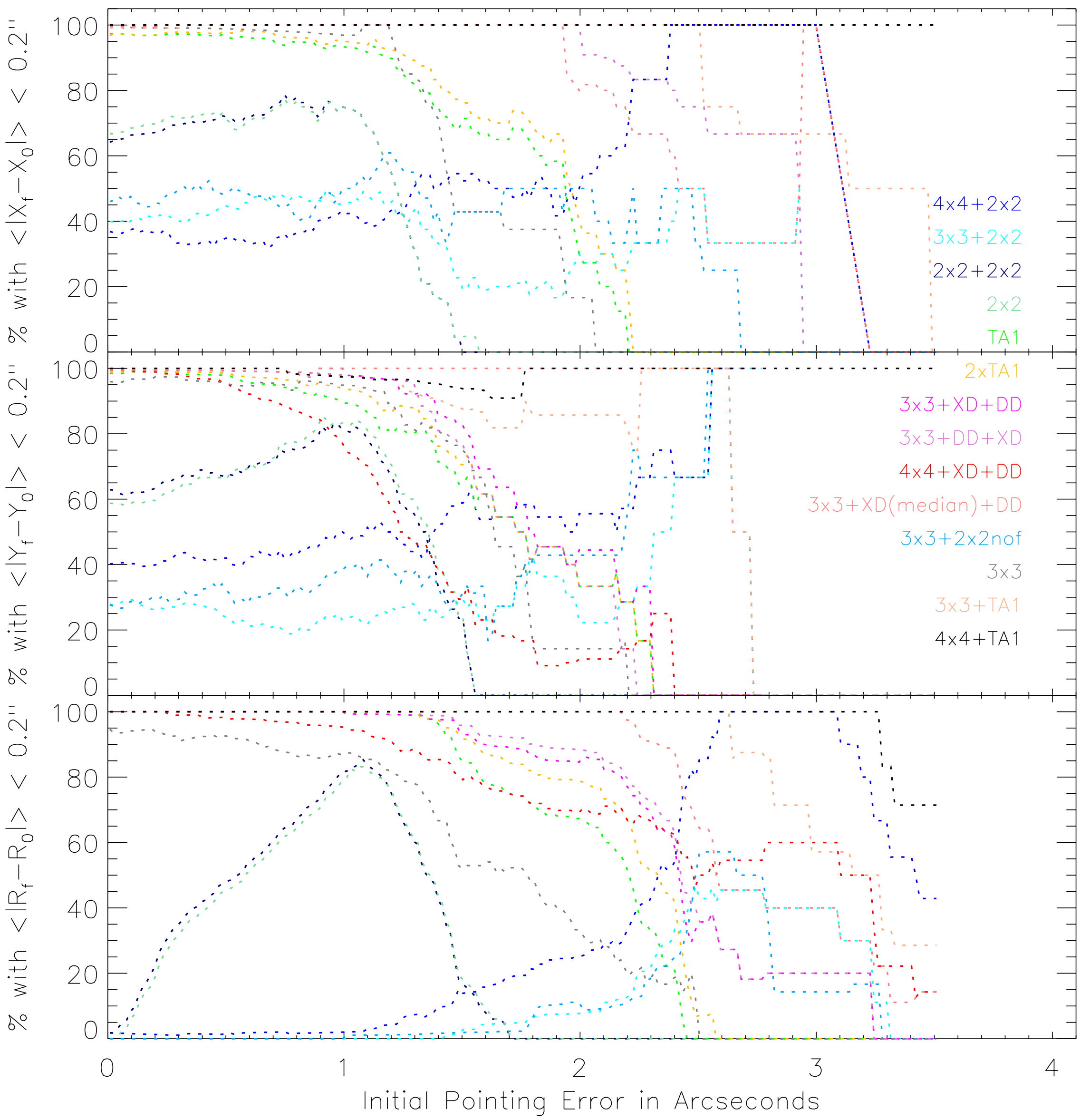

Figure 21: Accuracy extents of the TA strategies for a 3σ=3" distribution. The left axis gives the percentage of targets acquired to within 0.08" for DD (top), XD (middle) and in radius (R, bottom). A one-arcsecond moving boxcar has been used to smooth the data. The DD and XD distribution of initial target positions (X_0 and Y_0) is shown in Figure 20, while the radial (R_0) distribution is shown in Figure 22.

6.1.1 TA STRATEGY COMPARISON OF DURATION AND DD ACCURACY

Overall TA accuracy must be balanced by total elapsed time to determine the best TA strategies. Since the DD centering accuracy is the important science driver, we focus on DD accuracy as a function of time for our fourteen TA scenarios. In Figure 22, we plot the percentage of target acquisitions that achieve a DD centering accuracy of < 0.08” versus the total elapsed time as predicted in the previous sections. The horizontal error bars represent the temporal extent for the three NUV gratings. The solid colored circles indicate the maximum expected TA time using our conservative (round up to the next minute at each phase) estimates. The vertical error bars are taken as the square root of the number of trials. The initial DD distribution is shown as the inset histogram of number (N) versus initial radial position (R_0). Only pointings with radial initial offsets with R_0<3” were considered in this comparison. In this comparison, for this DD distribution, the best TA strategies appear to be 3x3 LTASRCH+LTAIMAGE, 3x3 LTASRCH+ LTAPKXD+ LTAPKD, and the similar 4x4 strategies. The LTAIMAGE only strategies are much faster, but are not able to accurately center targets with R_0 > 1.75”.

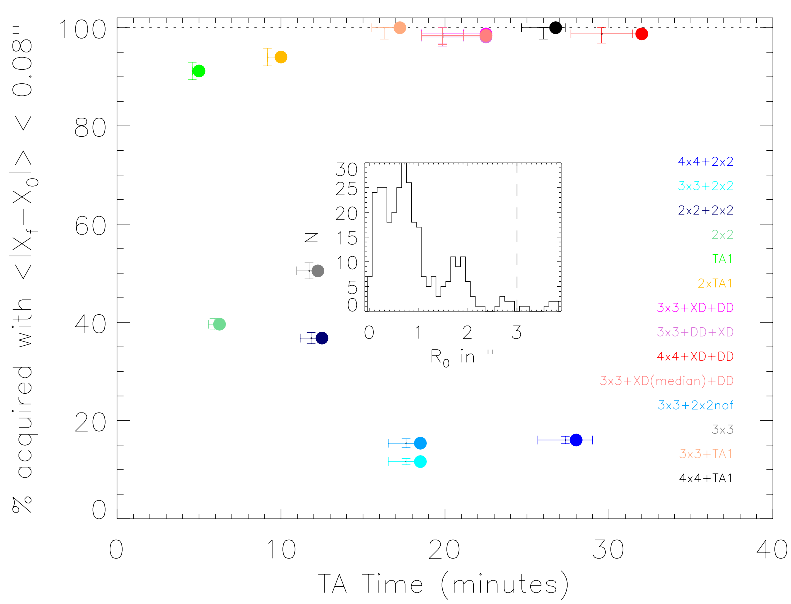

Figure 22: TA strategy summary for a 3σ=3" distribution, truncated at 3”. In this figure, only initial pointings with radial errors of R_0 < <3” are considered. Left axis gives the percentage of targets acquired to within 0.08” in the DD for the distribution shown in the inset histogram. Bottom axis gives the predicted total TA time in minutes. Horizontal error bars represent the temporal extent for the NUV gratings. Solid colored circles indicate the maximum expected TA time using our conservative estimates. Vertical error bars are based on the square root of the number of trials. The ideal TS strategy would be in the upper left.

COS observers will often know their target coordinates to accuracies higher than 3”. In Figure 23, we repeat the analysis of the previous figure, but for a 3σ=3" distribution that is truncated so that R_0<1.75”. For this distribution, the LTAIMAGE only TA strategies acquire 100% of target to DD errors of < 0.08”. Other strategies also acquire 100% of target to this DD accuracy, but typically take up to 10 times longer.

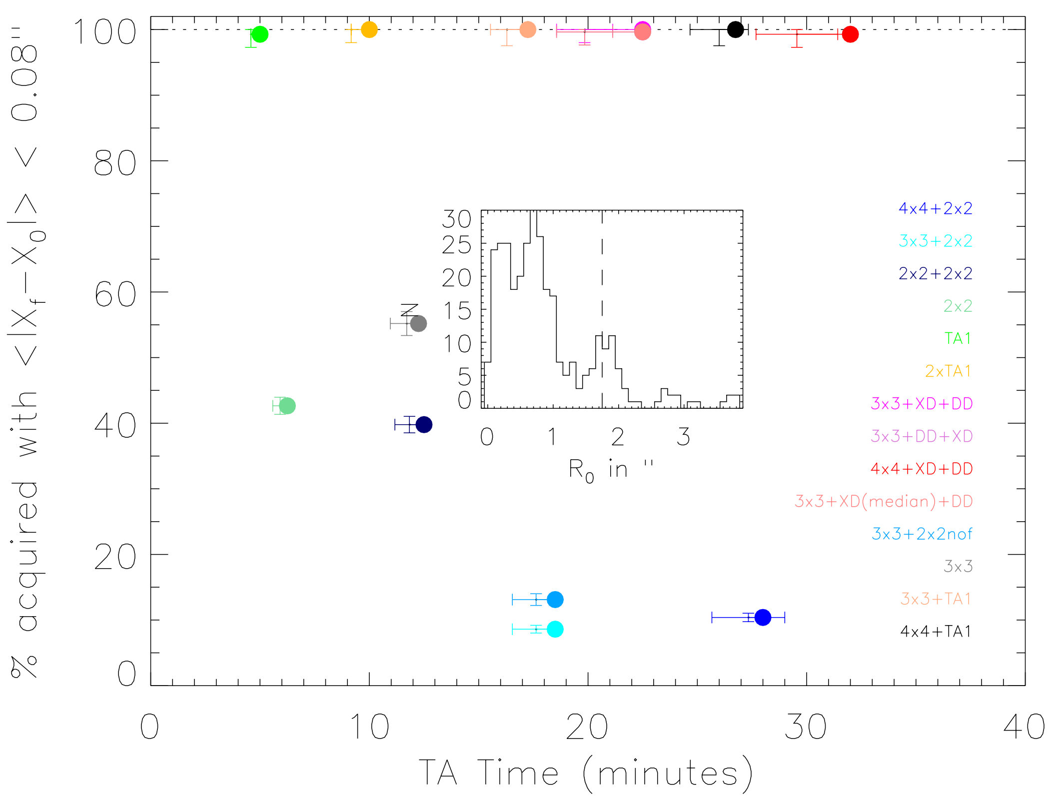

Figure 23: TA strategy summary for a 3σ=3" distribution, truncated at 1.75”. In this figure, only initial pointings with radial errors of R_0 <1.75” are considered. Left axis gives the percentage of targets acquired to within 0.08” in the DD for the distribution shown in the inset histogram. Bottom axis gives the predicted total TA time in minutes. Horizontal error bars represent the temporal extent for the NUV gratings. Solid colored circles indicate the maximum expected TA time using our conservative estimates. Vertical error bars are based on the square root of the number of trials. The ideal TS strategy would be in the upper left.

7. SUMMARY

The goal of the TAACOS NUV project was to determine if the proposed target acquisition (TA) algorithms were sufficient to center an isolated point source in the COS PSA to within 0.24” (preferably 0.08”). We find that the proposed procedures are adequate for this task, provided slight modifications to the procedures are installed. With these modifications, TAs should be able to acquire targets to within 0.24” in both dispersion (DD) and cross-dispersion (XD) in the 3σ case for sufficiently small initial pointing offsets. In the majority of cases, the final pointing errors will be < 0.08”. As shown in Equation 4 below, a 0.1” DD pointing offset equates to a TA introduced 3σ wavelength error of <19 km/s for the medium resolution gratings, and <200 km/s for the G230L. Standard TAs should take less than 30 minutes. All results described here are for a $F_{\lambda}=10^{-14}$ ergs/cm^2/s/Å QSO spectrum observed for 20s with the G230L and 30s with the medium resolution gratings.

The major findings of the report are:

- The higher background rate of the NUV MAMA mandates that a “floored” threshold flux centroid (FFC) algorithm be used. COS-11-0021 will provide the details of this algorithm. The FFC algorithm should be used during the NUV LTASRCH and LTAPKD procedures.

- Extraction subarrays are required for all phases of NUV TA due to the detector background.

- Due to the overlap of the NUV spectral stripes, LTASRCH and LTPKD should use a single large TA extraction subarray.

- Extraction subarrays that remove Geocoronal airglow lines are not essential for NUV TA. We do not see a need for moving extraction subarrays, which account for the motion of the target spectrum in the DD with motion in the aperture.

- Unlike the FUV, double spiral searches are not effective for NUV TA due to the higher background rate of the MAMA.

- Use of the TA1 mirror for target acquisition (LTAIMAGE) appears to be an extremely fast and accurate TA option, provided care is taken to avoid overilluminating the detector.

- The target must be centered to within ±0.65” for LTAPKXD to succeed. Use of the mean XD value produced only marginal XD centering to the very low S/B

(1.2) of the test TA used in this report ($F_\lambda=10^{-14}$ ergs/cm^2/s/Å QSO spectrum). The median XD coordinate produced much better results than the mean. However, when combined with a LTASRCH and LTAPKD, the mean algorithm produces acceptable results.

- For initial pointing errors less than 3" the best standard TA appears to a 3x3x1.767" LTASRCH followed by a LTAPKXD and a LTAPKD. A median algorithm for LTAKPKD would be preferable, but the mean may be acceptable. For LTAPKD, the appropriate number of dwell points appears to be five. This strategy should take ~20 minutes. However, for larger initial pointing errors a 4x4x1.767" would increase the sky area searched in ~28 minutes.

- For initial pointing errors less than 1.75", LTAIMAGE are clearly the best option. Depending on the S/N of the TA exposure, centering accuracies of <0.01" are achievable.

- Due to the magnitude of the plate scale cross-term α_{yy}, it is recommended that the LTAPKXD procedure be performed before the LTAPKD. The LTAPKD procedure will move the target in the ACS X direction, but will not move the target in DCS X.

Equation 4: Velocity equivalents of TA errors

$$\Delta v(G185M\,@1825\AA) = c * \frac{\left(0.1'' * {}^{42.47p}\!/\!_{''} * {}^{25\mu m}\!/\!_{p} * {}^{28\AA}\!/\!_{25.6mm}\right)}{1825\AA} = 19 km/s \quad (0.11\AA)$$

$$\Delta v(G225M\,@2250\AA) = c * \frac{\left(0.1'' * {}^{42.47p}\!/\!_{''} * {}^{25\mu m}\!/\!_{p} * {}^{35\AA}\!/\!_{25.6mm}\right)}{2250\AA} = 19 km/s \quad (0.15\AA)$$

$$\Delta v(G285M\,@2850\AA) = c * \frac{\left(0.1'' * {}^{42.47p}\!/\!_{''} * {}^{25\mu m}\!/\!_{p} * {}^{41\AA}\!/\!_{25.6mm}\right)}{2850\AA} = 18 km/s \quad (0.17\AA)$$

$$\Delta v(G230L\,@2450\AA) = c * \frac{\left(0.1'' * {}^{42.47p}\!/\!_{''} * {}^{25\mu m}\!/\!_{p} * {}^{398\AA}\!/\!_{25.6mm}\right)}{2450\AA} = 200 km/s \quad (1.65\AA)$$